Transition of streamwise streaks in zero-pressure-gradient boundary layers

By LUCA BRANDT AND DAN S. HENNINGSON†

Department of Mechanics, Royal Institute of Technology (KTH), S-100 44 Stockholm, Sweden

A transition scenario initiated by streamwise low- and high-speed streaks in a flat-plate boundary layer is studied. In many shear flows, the perturbations that show the highest potential for transient energy amplification consist of streamwise-aligned vortices. Due to the lift-up mechanism these optimal disturbances lead to elongated streamwise streaks downstream, with significant spanwise modulation. In a previous investigation (Andersson *et al.* 2001), the stability of these streaks in a zero-pressure-gradient boundary layer was studied by means of Floquet theory and numerical simulations. The sinuous instability mode was found to be the most dangerous disturbance. We present here the first simulation of the breakdown to turbulence originating from the sinuous instability of streamwise streaks. The main structures observed during the transition process consist of elongated quasi-streamwise vortices located on the flanks of the low-speed streak. Vortices of alternating sign are overlapping in the streamwise direction in a staggered pattern. The present scenario is compared with transition initiated by Tollmien–Schlichting waves and their secondary instability and by-pass transition initiated by a pair of oblique waves. The relevance of this scenario to transition induced by free-stream turbulence is also discussed.

1. Introduction

1.1. *Natural transition*

Transition from laminar to turbulent flow has traditionally been studied in terms of exponentially growing eigensolutions to the linearized disturbance equations. Equations for the evolution of a disturbance, linearized around a mean velocity profile were first derived by Lord Rayleigh (1880) for an inviscid flow; later Orr (1907) and Sommerfeld (1908) included the effects of viscosity, deriving independently what we today call the Orr–Sommerfeld equation. Assuming a wave-like form of the velocity perturbation and Fourier transforming, the equation reduces to an eigenvalue problem for exponentially growing or decaying disturbances. The first solutions for unstable waves, travelling in the direction of the flow (two-dimensional waves), were presented by Tollmien (1929) and Schlichting (1933). The existence of such solutions (later called Tollmien–Schlichting waves) was experimentally verified by Schubauer & Skramstad (1947) in a zero-pressure-gradient boundary layer.

If an amplified Tollmien–Schlichting wave grows above an amplitude in u_{rms} of about 1% of the free-stream velocity, the flow become susceptible to secondary instability. Klebanoff, Tidstrom & Sargent (1962) observed that three-dimensional

† Also at FOI, The Swedish Defense Research Agency, Aeronautics Division, SE-17290 Stockholm, Sweden.

perturbations, which are present in any natural flow, were strongly amplified. The three-dimensional structure of the flow was characterized by regions of enhanced and diminished perturbation velocity amplitudes alternating in the spanwise direction, denoted by them 'peaks and valleys'. The spanwise scale of the new pattern was of the same order as the streamwise wavelength of the Tollmien–Schlichting (TS) waves and the velocity time signal showed the appearance of high-frequency disturbance spikes at the peak position. This transition scenario was later denoted as K-type after Klebanoff and also fundamental since the frequency of the secondary, spanwise-periodic, fluctuations is the same as that of the TS-waves. In the nonlinear stages of the K-type scenario, rows of 'Λ-shaped' vortices, aligned in the streamwise direction, have been observed. Another scenario was also observed, first by Kachanov, Kozlov & Levchenko (1977). This is denoted N-type after Novosibirsk, where the experiments were carried out or H-type after Herbert, who performed a theoretical analysis of the secondary instability of TS-waves (Herbert 1983). In this scenario, the frequency of the secondary instability mode is half that of the TS-waves and, thus, this is also known as subharmonic breakdown. 'Λ-shaped' vortices are also present in this case, but they are arranged in a staggered pattern. Theoretically, this scenario is more likely to occur than the fundamental or K-type, because of its higher growth rate for TS amplitudes of the order of 1% of the free-stream velocity. The temporal calculations by Spalart & Yang (1987) also showed that this was the case. In experiments, however, K-type is often seen in many cases where H-type is theoretically favoured, due to the presence of low-amplitude streamwise vorticity in the background flow (Herbert 1988). A review on the physical mechanisms involved can be found in Kachanov (1994).

Transition originating from exponentially growing eigenfunctions is usually called *classical* or *natural* transition. This is observed naturally in flows only if the background turbulence is very small. For higher values, the disturbances inside the boundary layer are large enough that other mechanisms play an important role and the natural scenario is by-passed.

1.2. By-pass transition

1.2.1. Transient growth of streamwise streaks

In 1969 Morkovin coined the expression 'by-pass transition', noting that 'we can by-pass the TS-mechanism altogether'. In fact, experiments reveal that many flows, including channel and boundary layer flows, may undergo transition for Reynolds numbers well below the critical ones from linear stability theory. Ellingsen & Palm (1975) proposed a growth mechanism, considering the inviscid evolution of an initial disturbance independent of the streamwise coordinate in a shear layer. These authors showed that the streamwise velocity component may grow linearly in time, producing alternating low- and high-velocity streaks. Moffatt (see the review article by Phillips 1969) also identified such a streak growth mechanism in a model of turbulent uniform shear flow. Later Hultgren & Gustavsson (1981) considered the temporal evolution of a three-dimensional disturbance in a boundary layer and found that in a viscous flow the initial growth is followed by a viscous decay (*transient growth*).

Landahl (1975, 1980) extended this result to the linear evolution of localized disturbances and formalized a physical explanation for this growth. A wall-normal displacement of a fluid element in a shear layer will cause a perturbation in the streamwise velocity, since the fluid particle will initially retain its horizontal momentum. It was observed that weak pairs of quasi-streamwise counter-rotating vortices are

able to lift up fluid with low velocity from the wall and bring high-speed fluid towards the wall, and so they are the most effective in forcing streamwise-oriented streaks of high and low streamwise velocity. This mechanism, denoted the *lift-up effect*, is inherently a three-dimensional phenomenon. Some insight into it may also be gained from the equation for the wall-normal vorticity of the perturbation (the Squire equation), which is proportional to the streamwise velocity for streamwise-independent disturbances. The equation is, in fact, forced by a term due to the interaction between the spanwise variation of the wall-normal velocity perturbation and the mean shear of the base flow.

From a mathematical point of view, it is now clear that since the linearized Navier–Stokes operator is non-normal for many flow cases (e.g. shear flows), a significant transient growth may occur before the subsequent exponential behaviour (see Butler & Farrell 1992; Reddy & Henningson 1993; Schmid & Henningson 2001). Such growth is larger for disturbances mainly periodic in the spanwise direction, i.e. with low streamwise wavenumbers in a temporal formulation or low frequency in a spatial one; it can exist for sub-critical values of the Reynolds number and it is the underlying mechanism in by-pass transition phenomena. Andersson, Berggren & Henningson (1999) and Luchini (2000) used an optimization technique to determine which disturbance present at the leading edge of a flat plate will give the maximum spatial transient growth in a non-parallel boundary layer. They also found a pair of counter-rotating streamwise vortices as the most effective in streak's generation.

One of the most interesting cases in which disturbances originating from non-modal growth are responsible for transition is in the presence of free-stream turbulence. Inside the boundary layer the turbulence is highly damped, but low-frequency oscillations, associated with long streaky structures, appear. The effect of free-stream streamwise vorticity on a laminar boundary layer is studied in Wundrow & Goldstein (2001). As the streaks grow downstream, they break down into regions of intense randomized flow, turbulent *spots*. Experiments with flow visualizations by for example Matsubara & Alfredsson (2001) report on the presence of a high-frequency 'wiggle' of the streak before the subsequent breakdown into a turbulent spot. Numerical simulations of a transitional boundary layer under free-stream turbulence are presented in Jacobs & Durbin (2001).

Another case where transient growth plays an important role is in the so-called *oblique transition*. In this scenario, streamwise-aligned vortices are generated by non-linear interaction between a pair of oblique waves with equal angle but opposite sign in the flow direction. These vortices, in turn, induce streamwise streaks, which may grow past a certain amplitude and become unstable, initiating the breakdown to a turbulent flow. Oblique transition has been studied in detail by Schmid & Henningson (1992) and Elofsson & Alfredsson (1998) in a channel flow and both numerically and experimentally by Berlin, Wiegel & Henningson (1999) for a boundary layer flow.

1.2.2. *Secondary instability of streaks*

If the disturbance energy of the streaks becomes sufficiently large, secondary instability can take place and provoke early breakdown and transition, overruling the theoretically predicted modal decay. Carefully controlled experiments on the breakdown of streaks in channel flow were conducted by Elofsson, Kawakami & Alfredsson (1999). They generated elongated streamwise streaky structures by applying wall suction, and triggered a secondary instability by the use of earphones. They observed that the growth rate of the secondary instability modes was unaffected by

a change of the Reynolds number of their flow and that the instability appeared as spanwise (sinuous-type) oscillations of the streaks in cross-stream planes. For numerical/theoretical studies on the instability in channel flows the reader is referred to the works of Waleffe (1995, 1997) and Reddy *et al.* (1998). Flow visualizations of the instability and breakdown of a near-wall low-speed streak in a boundary layer can be found in the recent experiments by Asai, Minagawa & Nishioka (1999, 2002).

In Andersson *et al.* (2001), direct numerical simulations (DNS) were used to follow the nonlinear saturation of the optimally growing streaks in a spatially evolving zero-pressure-gradient boundary layer. The complete velocity vector field from the linear results by Andersson *et al.* (1999) was used as input close to the leading edge and the downstream nonlinear development monitored for different initial amplitudes of the perturbation. Inviscid secondary instability calculations using Floquet theory were performed on the mean flows obtained and it was found that the streak critical amplitude, beyond which streamwise travelling waves are excited, is about 26% of the free-stream velocity. The sinuous instability mode (either the fundamental or the subharmonic, depending on the streak amplitude) represents the most dangerous disturbance. Varicose waves are more stable, and are characterized by a critical amplitude of about 37%.

In the present paper we study the transition process resulting from the sinuous secondary instability using DNS. The late stages of the process are investigated and flow structures identified. This is the first numerical study which accounts in detail for the sinuous breakdown of streaks in boundary layers.

The paper is organized as follows. After an introduction in §2, where the numerical method employed is described, the features of this novel scenario are presented in §3. In §4 this is compared with the other well-known transition scenarios, such as transition initiated by TS-waves, pairs of oblique waves and transition due to free-stream turbulence. In addition there is a discussion regarding the relevance of the reported results in the description of the dynamics of near-wall turbulent streaks. The main conclusions of the paper are summarized in §5.

2. Numerical method

2.1. *Numerical scheme*

The simulation code (see Lundbladh *et al.* 1999) employed for the present computations uses spectral methods to solve the three-dimensional, time-dependent, incompressible Navier–Stokes equations. The algorithm is similar to that of Kim, Moin & Moser (1987), i.e. Fourier representation in the streamwise and spanwise directions and Chebyshev polynomials in the wall-normal direction, together with a pseudo-spectral treatment of the nonlinear terms. The time advancement used is a four-step low-storage third-order Runge–Kutta method for the nonlinear terms and a second-order Crank–Nicolson method for the linear terms. Aliasing errors from the evaluation of the nonlinear terms are removed by the $\frac{3}{2}$-rule when the FFTs are calculated in the wall-parallel plane. In the wall-normal direction it has been found more efficient to increase resolution rather than using dealiasing.

To correctly account for the downstream boundary layer growth a spatial technique is necessary. This requirement is combined with the periodic boundary condition in the streamwise direction by the implementation of a 'fringe region', similar to that described by Bertolotti, Herbert & Spalart (1992). In this region, at the downstream end of the computational box, the function $\lambda(x)$ in equation (2.1) is smoothly raised

from zero and the flow is forced to a desired solution v in the following manner:

$$\frac{\partial \boldsymbol{u}}{\partial t} = NS(\boldsymbol{u}) + \lambda(x)(\boldsymbol{v} - \boldsymbol{u}) + \boldsymbol{g}, \tag{2.1}$$

$$\nabla \cdot \boldsymbol{u} = 0, \tag{2.2}$$

where $\boldsymbol{u}$ is the solution vector and $NS(\boldsymbol{u})$ the right-hand side of the (unforced) momentum equations. Both $\boldsymbol{g}$, which is a disturbance forcing, and $\boldsymbol{v}$ may depend on the three spatial coordinates and time. The forcing vector $\boldsymbol{v}$ is smoothly changed from the laminar boundary layer profile at the beginning of the fringe region to the prescribed inflow velocity vector. This is normally a boundary layer profile, but can also contain a disturbance. A convenient form of the fringe function is as follows:

$$\lambda(x) = \lambda_{max} \left[S \left(\frac{x - x_{start}}{\Delta_{rise}} \right) - S \left(\frac{x - x_{end}}{\Delta_{fall}} + 1 \right) \right], \tag{2.3}$$

where λ_{max} is the maximum strength of the damping, x_{start} to x_{end} the spatial extent of the region where the damping function is non-zero and Δ_{rise} and Δ_{fall} the rise and fall distance of the damping function. $S(a)$ is a smooth step function rising from zero for negative a to one for $a \geqslant 1$. We have used the following form for S, which has the advantage of having continuous derivatives of all orders.

$$S(a) = \begin{cases} 0, & a \leqslant 0 \\ 1 / \left[1 + \exp \left(\frac{1}{a - 1} + \frac{1}{a} \right) \right], & 0 < a < 1 \\ 1, & a \geqslant 1. \end{cases} \tag{2.4}$$

This method damps disturbances flowing out of the physical region and smoothly transforms the flow to the desired inflow state, with a minimal upstream influence.

In order to set the free-stream boundary condition at some $y = y_{max}$ closer to the wall, a generalization of the boundary condition used by Malik, Zang & Hussaini (1985) is implemented. Since it is applied in Fourier space with different coefficients for each wavenumber, it is non-local in physical space and takes the following form:

$$\frac{\partial \hat{\boldsymbol{u}}}{\partial y} + |k| \hat{\boldsymbol{u}} = \frac{\partial \hat{\boldsymbol{v}}_0}{\partial y} + |k| \hat{\boldsymbol{v}}_0, \tag{2.5}$$

where k is the absolute value of the horizontal wavenumber vector and $\hat{\boldsymbol{u}}$ is the Fourier transforms of $\boldsymbol{u}$. Here $\boldsymbol{v}_0$ denotes the local solution of the Blasius equation and $\hat{\boldsymbol{v}}_0$ its Fourier transform.

2.2. *Disturbance generation and parameter setting*

The presented numerical implementation provides several possibilities for disturbance generation. The velocity vector field from the simulations presented in Andersson *et al.* (2001, figure 9), is used as inflow condition. In those simulations a spanwise antisymmetric harmonic volume force was added to the nonlinear streaks to trigger their sinuous secondary instability. Here the saturated streaks, $\boldsymbol{v}_s$, and the secondary instability mode, $\boldsymbol{v}_d$, obtained by filtering the velocity field at the frequency ω of the forcing, are introduced in the fringe region by adding them to the Blasius solution to give the forcing vector $\boldsymbol{v} = \boldsymbol{v}_0 + \boldsymbol{v}_s + A\boldsymbol{v}_d \mathrm{e}^{\mathrm{i}\omega t}$ in equation (2.1). An amplification factor A is used for the secondary instability to give transition within the computational box, in the present case $A = 10^3$. The analysis of the fringe region technique by Nordström, Nordin & Henningson (1999) shows that no error is introduced in the simulations if

	$xl \times yl \times zl$ δ_0^*	$nx \times ny \times nz$ (resolution)	$Re_{\delta_0^*}$
Box1	$380 \times 10.7 \times 6.86$	$1024 \times 97 \times 96$	875
Box2	$380 \times 10.7 \times 6.86$	$1440 \times 97 \times 72$	875
Box3	$318 \times 9 \times 5.75$	$1440 \times 97 \times 72$	1044

TABLE 1. Resolution and box dimensions for the simulations presented. The box dimensions include the fringe region, and are made dimensionless with respect to δ_0^*, the displacement thickness at the beginning of the computational box. Note that zl corresponds in all cases to one spanwise wavelength of the streak. The total number of Fourier modes is indicated, corresponding to $nx/2$ or $nz/2$ conjugate pairs.

x	y	ω_z	$\Delta x/\lambda_x$	$\Delta y/3\delta_0^*$	$\Delta\omega_z/\omega_z$
205.60	1.57	−0.74	0.013	0.009	−0.013
210.51	1.2	−0.80	0.022	0.009	−0.008
215.86	0.8	−0.86	0.018	0.008	0.01
222.62	3.33	−0.66	0.00	0.043	0.0085
222.92	1.01	−1.42	0.021	0.033	0.0032
228.02	1.17	−1.45	0.034	0.053	0.0523
234.23	1.94	−0.86	0.008	0.00	0.02
238.64	2.74	−0.88	0.00	0.033	0.0054
247.39	0.93	−1.71	0.005	0.009	0.045

TABLE 2. Position of some local minima of the spanwise vorticity for the simulation with Box2 and the relative error with the same minima for the simulation with Box1. The difference in the y position is divided by $3\delta_0^*$, the length of the structure in the wall-normal direction, while the difference in the x position is related to the streamwise wavelength of the secondary instability mode ($\lambda_x = 11.9\delta_0^*$).

the forcing is a solution to the Navier–Stokes equations. This is true in the present case since the forcing vector is the result of previous direct numerical simulations performed by means of the same numerical code.

The box sizes and resolutions used for the simulations presented in this paper are displayed in table 1. The dimensions are reported in terms of δ_0^* which denotes the Blasius boundary layer displacement thickness at the beginning of the computational box. Box1 and Box2 follow the evolution of the secondary instability mode from the same upstream station and differ only in the number of spectral modes. Box3 has a larger inlet Re and is used to provide some fully developed turbulence within the computational box with a still feasible number of modes; the inflow of Box3 corresponds to $x = 125$ in Box1 and Box2. If not stated otherwise, in the results presented the coordinates will be scaled with the displacement thickness δ_0^* of Box1 and Box2. The inflow position $x = 0$, $Re = 875$ in the present paper corresponds to $x/L = 1.03$ in figure 9 in Andersson *et al.* (2001).

A check on the resolution of the present simulations is obtained comparing the minima of the spanwise vorticity component in the transition region obtained using Box1 and Box2. The data, extracted at the same phase angle during the period of the secondary instability mode, are reported in table 2 while the isocontours of the instantaneous spanwise vorticity are displayed in figure 1 in the (x, y)-plane located at the centre of the low-speed region ($z = 0$). The difference in the y position of the minima considered is divided by $3\delta_0^*$, the length of the structure in the wall-normal direction, while the difference in the x position is related to the streamwise wavelength
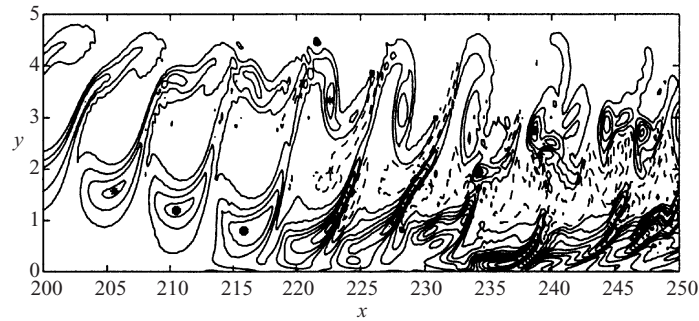
FIGURE 1. Isocontours of the instantaneous spanwise vorticity component at $z = 0$, $Re_{\delta_0^*} = 875$. Contour levels: minimum -2.1, maximum 0.7, spacing 0.2 (dashed lines, negative values). The black dots represent the points reported in table 2.
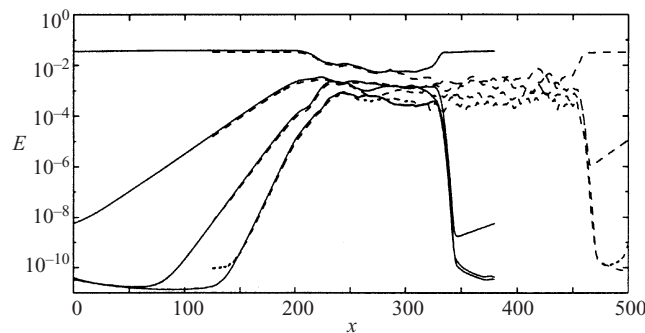

FIGURE 2. Energy in four different modes $(\omega, \beta) = (0, 1)$, $(1, 1)$, $(2, 1)$ and $(3, 1)$, from two different simulations: ——, Box2; - - - -, Box3. The effect of the fringe region can be seen.

of the secondary instability mode ($\lambda_x = 11.9\delta_0^*$). The maximum of the difference in the vorticity field between the two simulations is less than 6% for values of x less than 250. This is a first confirmation that the periodicity of the flow is maintained for x positions upstream of 250.

The resolution of Box3 is the same as Box2 in the y- and z-directions, while it is slightly increased in the streamwise variable. To show that in the Box3 simulation we are following the same phenomena from a position further downstream, the energy in the different Fourier modes is compared with that obtained using Box2 in figure 2. Sixteen velocity fields are saved during one period of the secondary instability mode. These velocity fields are then transformed in time and in the spanwise direction to Fourier space and the notation (ω, β), where ω and β are the frequency and spanwise wavenumber, each normalized with the corresponding fundamental frequency and wavenumber, is used. The same behaviour is observed for $x \lesssim 250$; hence we can assume that the resolution is adequate also for the simulation with Box3, as confirmed by plots of the energy spectra (not reported here). The evolution of the perturbation in the fringe region can also be seen in figure 2: both in Box2 and Box3 the fringe is 60 units long, therefore one can estimate that the x interval not affected by the fringe technique extends up to $x \approx 310$ and $x \approx 445$ respectively (see Nordström *et al.* 1999, for the analysis of the upstream influence of the fringe region).
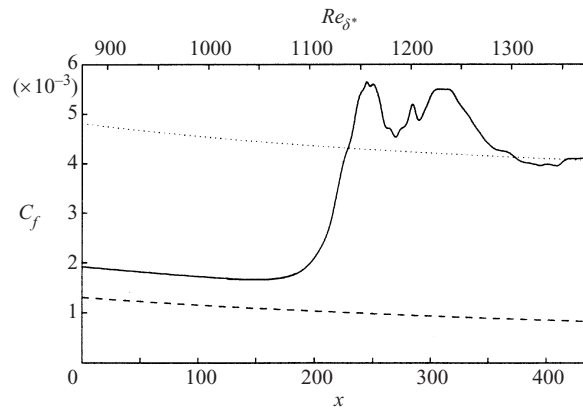
FIGURE 3. Skin friction coefficient versus the streamwise position. Both the streamwise variable x used throughout the paper and the corresponding Reynolds number based on the local Blasius displacement thickness are displayed. ——, Present simulations; - - - -, laminar values; $\cdots$, turbulent coefficient according to the Prandtl–Schlichting formula.

3. Results

In the first part of this section we give an overview of the full transition scenario of a streamwise streak subjected to sinuous secondary instability. Instantaneous flow structures and mechanisms responsible for the breakdown are discussed in § 3.4. In § 4 we compare this new scenario with other known transition senarios.

3.1. *Friction coefficient and predictability*

The skin friction coefficient is shown in figure 3 versus the streamwise location; it is obtained by averaging in time and in the spanwise direction. Also, the values for a Blasius laminar flow and a turbulent boundary layer are displayed for comparison. C_f starts to rise at $x \approx 190$ and reaches two maxima at $x \approx 250$ and $x \approx 310$. The streamwise location of maximum skin friction may be used to define the completion of the transition process, and in fact, as will be shown in the next section, the flow starts to lose its predictability and periodicity at $x \approx 250$. Strong streaks are already present at the beginning of the simulations, therefore the value of C_f is higher than in the laminar case. The increase in wall shear stress is due to the nonlinear modification of the mean velocity profile which is positive close to the wall and becomes negative for higher y, see figure 13 in Andersson *et al.* (2001).

A characteristic of turbulent flows is its unpredictability. In fact two flows, initially very close, will become completely uncorrelated as time goes on. Before discussing the flow characteristics, we need to determine for which downstream positions the flow may still be considered deterministic, i.e. determined by the periodic inflow conditions, and where instead it can be seen as randomized. This would give us a further indication of the transition location and help in identifying the flow structures fundamental in the transition process.

A quantitative measure of the aperiodicity and loss of predictability can be defined by a functional g, given by

$$g(f) = \log_{10} \left[\frac{1}{N} \sum (f(t) - f(t+mT))^2 \right]^{1/2},$$

where $f(t)$ and $f(t+mT)$ are the values of a quantity f at time t and after an integer
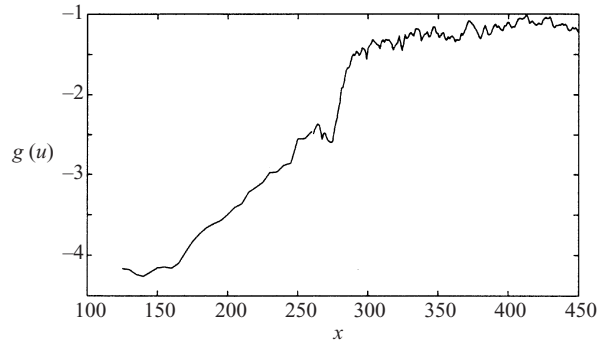
FIGURE 4. The aperiodicity measure g for the streamwise velocity component u, showing the loss of predictability during the transition process.

number m of periods (T), and the summation is over the $N = N_y \times N_z$ points defining an (y, z)-plane. In Sandham & Kleiser (1992) the authors define a similar quantity for the case of temporal simulations of transition in a channel flow originating from secondary instability of Tollmien–Schlichting waves. In that case the loss of symmetry between the two halves of the channel is considered as time evolves. In our spatial simulations the loss of time periodicity at the different x positions is studied as the disturbance travels downstream.

The values of g obtained from the streamwise velocity component are shown in figure 4. Expressing the growth of the aperiodicity as $e^{\sigma x}$, we can interpolate the data to obtain a value of $\sigma = 0.016$ for $x < 240$, which is comparable with the growth of the energy $\sigma_e = 2\sigma_u = 0.033$ of the secondary instability mode obtained from the data shown in figure 2. In this region the flow is governed by the growth of the secondary instability modes, so if a difference is present in two initial conditions it will grow as the secondary instability itself. The loss of predictability occurs very late in the transition process, noticed by the sharp change of slope at $x \approx 250$. This result is consistent with the location of maximum skin friction. At this location the Reynolds numbers based on the friction velocity u_τ and the momentum loss thickness or the boundary layer thickness δ_{99} are respectively $Re_{\tau,\theta} \approx 35$ and $Re_{\tau,\delta_{99}} \approx 240$. For $x \approx 300$ the decorrelation becomes larger and then stays constant with the downstream position.

3.2. Spectral analysis and eigenmode structure

3.2.1. Development of Fourier components

The energy in some time and spanwise Fourier modes is displayed in figure 5, where the zero frequency mode represents the streak. The secondary instability mode ($\omega = 1$) is present at the beginning of the computation, while the higher harmonics are excited as the flow evolves downstream (compare figure 2). The energy growth is exponential for a long streamwise distance and the growth rate of the first harmonic ($\omega = 2$) is twice that of the fundamental secondary instability and similarly for higher frequencies the growth rate is proportional to the harmonic order. This is a consequence of the fact that the first harmonic is forced by nonlinear interactions of the fundamental mode and so its exponential behaviour is given by the sum of those of the interacting modes. In the same way the mode with $\omega = 3$ is induced by the interaction of $\omega = 1$ and $\omega = 2$ modes and it is characterized by a growth rate that is about $3\sigma_e$. It is interesting to note that the energy content is of the same order
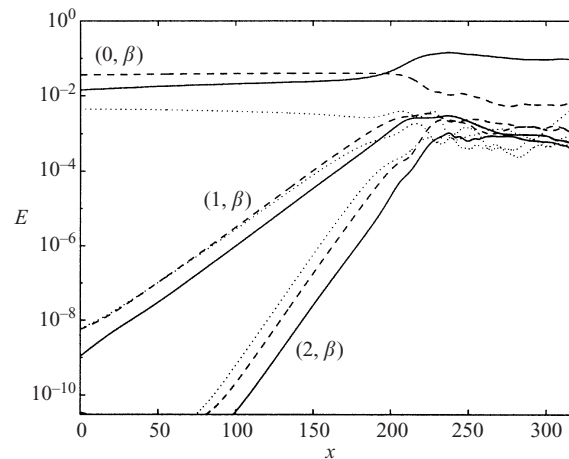
FIGURE 5. Energy in different Fourier modes (ω, β) versus the streamwise position. Frequencies: zero (streaks), one (secondary instability), two (higher harmonic). ——, $\beta = 0$; ----, $\beta = 1$; $\cdots\cdots$, $\beta = 2$.

for modes with different spanwise wavenumbers but with the same frequency. This result is different from the one obtained when the same analysis is applied to a case of transition initiated by two oblique waves (see Berlin *et al.* 1999) or by Tollmien–Schlichting waves (see Laurien & Kleiser 1989; Rist & Fasel 1995, for example). In these cases nonlinear interactions are important to select the modes dominating the transition process, namely the streamwise-independent ones, while here streaks are induced from the start and they develop to a highly nonlinear stage before they become unstable to time-dependent disturbances; thus the harmonics in the spanwise direction are generated during the streak growth and are responsible for the large spanwise shear of the flow. The instability of such a flow is then characterized by modes strongly localized in the spanwise direction so that a number of wavenumbers β is needed to correctly capture them (see Andersson *et al.* 2001).

The growth in the different harmonics starts to saturate around position $x = 200$ and soon the energy becomes of the same order for the different ω values. From this point ($x \approx 220$) the Fourier transform in time of the whole velocity fields is no longer accurate since not enough frequencies are resolved. In fact higher and higher harmonics are excited until the energy spectra fill out, with increasing values in a large low-frequency band, due to the now strong nonlinear interactions. Analysis of the time signal of the streamwise velocity fluctuations at different locations thus reveals some interesting features of the flow. In fact at positions further downstream of the transition point and in the outer part of the boundary layer the flow still maintains the dominating periodicity of the inflow perturbation, while close to the wall the time traces look random and completely uncorrelated to the secondary instability mode. A similar behaviour is observed in the natural transition scenario by Meyer *et al.* (1999). They noted, in fact, that the growth of some non-periodic random perturbation occurs in the near-wall region below the deterministic evolution of stable ring-like structures. Finally, some features of the mean flow can be assessed by looking at the different components of the stationary disturbance, in figure 5, i.e. $(0, \beta)$ modes, recalling that the $(0, 1)$ and $(0, 2)$ modes represent the spanwise modulation of the flow and $(0, 0)$ is the distortion from the Blasius profile. The energy in the first two decreases by a factor of ten as soon as the late stages of the transition process are reached, indicating
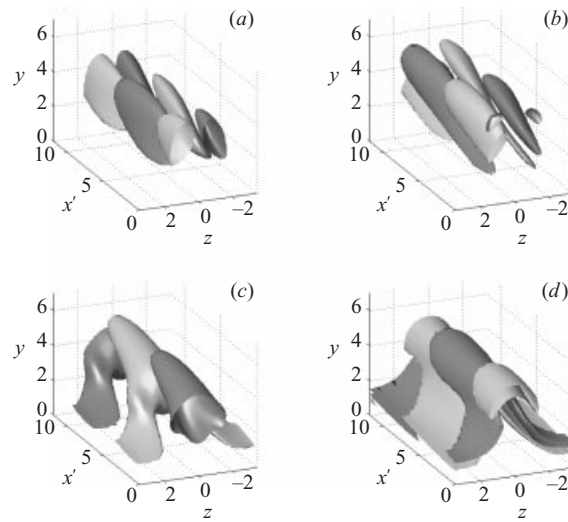
FIGURE 6. Isosurfaces of positive and negative values of the secondary instability eigenmode: (*a*) streamwise velocity component; (*b*) wall-normal velocity component; (*c*) spanwise velocity component; (*d*) streamwise vorticity component. The streamwise coordinate $x' = x - 125$ reflects the local view of the figure.

that the mean flow is losing its modulation, while the latter mode is growing since the mean laminar velocity profile is approaching its turbulent counterpart.

3.2.2. *Eigenmode structure and streamwise vorticity generation*

As observed in a number of experiments and numerical studies, see Swearingen & Blackwelder (1987) and LeCunff & Bottaro (1993) for example, the sinuous instability can be related to the spanwise inflectional points of the mean flow. Andersson *et al.* (2001) have shown that the streamwise velocity of the secondary instability modes is concentrated around the critical layer, i.e. the layer of constant value of the mean field velocity corresponding to the phase speed of the disturbance which is $u = 0.81 U_\infty$ in the present case, thus confirming the inviscid nature of the instability considered. In this work we extend the previous analysis to consider the complete three-dimensional structure of the eigenfunction in order to investigate the instability mechanism leading to the formation of streamwise vorticity.

A three-dimensional plot of the secondary instability mode is displayed in figure 6. This is obtained from the Fourier-transformed velocity fields discussed in §3.2.1, filtering at the fundamental frequency. The mode is characterized by a streamwise wavelength $\lambda_x = 11.9$ and a frequency $\omega = 0.43$; only one wavelength λ_x is shown in the plots around position $x = 125$. Isosurfaces of positive and negative streamwise and wall-normal velocity are plotted in figures 6(*a*) and 6(*b*) and show the odd symmetry of this kind of instability. The fluctuations are stronger around $z = 0$, i.e. in the low-speed region. The result is the spanwise oscillation of the low-speed streak. The spanwise velocity, seen in figure 6(*c*), is in fact characterized by alternating positive and negative values, with a symmetric distribution of the disturbance with respect to the streak. All the perturbation velocity components appear tilted towards the streamwise direction.

In figure 6(*d*) the streamwise disturbance vorticity is also shown. This is symmetric with respect to the streak; structures of the same sign appear above the low- and high-
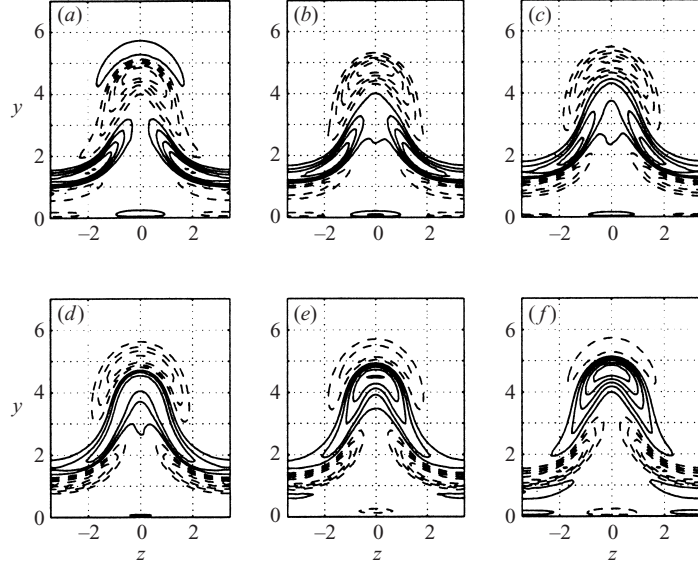
FIGURE 7. Streamwise vorticity of the secondary instability mode during half a period of the disturbance evolution at $x = 125$. From time $t = 1\,T/10$ to $t = 6\,T/10$ for (*a*) to (*f*). Contour levels: min 0.019, max 0.019, spacing 4×10^{-3}.

speed streak, connected by legs situated along the flanks of the low-speed region. In a similar manner to Kawahara *et al.* (1998) we analyse the production of streamwise vorticity for the unstable sinuous eigenfunction. Since the structures observed at the late stages of transition consist of elongated quasi-streamwise vortices, we focus our study on the streamwise component only. The streamwise vorticity of the base flow is initially very low so that its production is almost entirely related to the instability features. Analysis of the wall-normal and spanwise vorticity showed in fact that vorticity fluctuations are mainly induced by the periodic advection of the strong shear layers of the streaky base flow by the velocity fluctuations.

To derive an equation for the streamwise vorticity perturbation, we consider a parallel base flow, consisting at leading order only of the streamwise velocity component, i.e. $U = (U(y, z), 0, 0)$. This is shown in Andersson *et al.* (2001) to describe correctly the streak's instability. This yields

$$\left(\frac{\partial}{\partial t} + U \frac{\partial}{\partial x} \right) \omega_x = \frac{\partial U}{\partial z} \frac{\partial v}{\partial x} - \frac{\partial U}{\partial y} \frac{\partial w}{\partial x} + \frac{1}{Re} \nabla^2 \omega_x, \tag{3.1}$$

where the first two terms on the right-hand side represent vorticity production by vortex tilting and the third represents viscous dissipation, which we will neglect. The first of the two production terms is due to the tilting of the spanwise disturbance vorticity ($\partial v / \partial x$) by the spanwise shear ($\partial U / \partial z$), while the second represents the tilting of the wall-normal vorticity-perturbation ($\partial w / \partial x$) by the mean wall-normal shear ($\partial U / \partial y$). In figures 7, 8, 9 we display contour levels of the streamwise vorticity ω_x and of the two production terms at position $x = 125$ during half a period of the disturbance evolution, in such a way that the plot in the lower right-hand corner is the exact opposite of the one in the upper left-hand corner (or they have a phase difference of π). The wall-normal shear is larger than the spanwise shear; the former is largest in the regions above the high-speed streak while the latter is largest on the
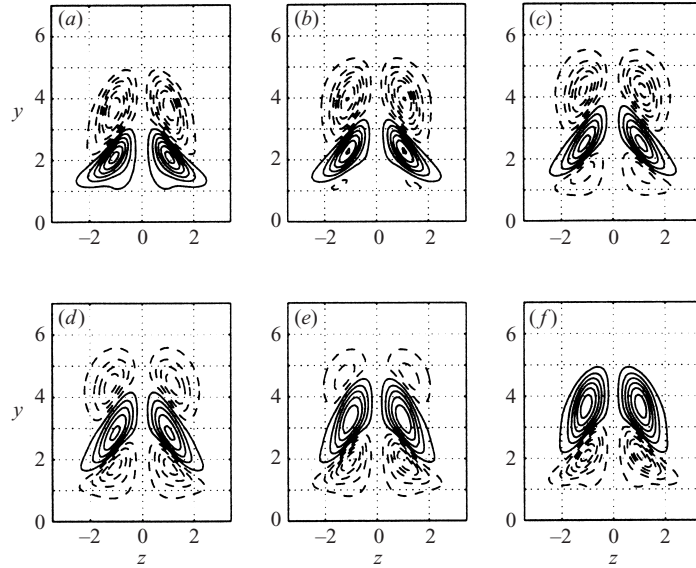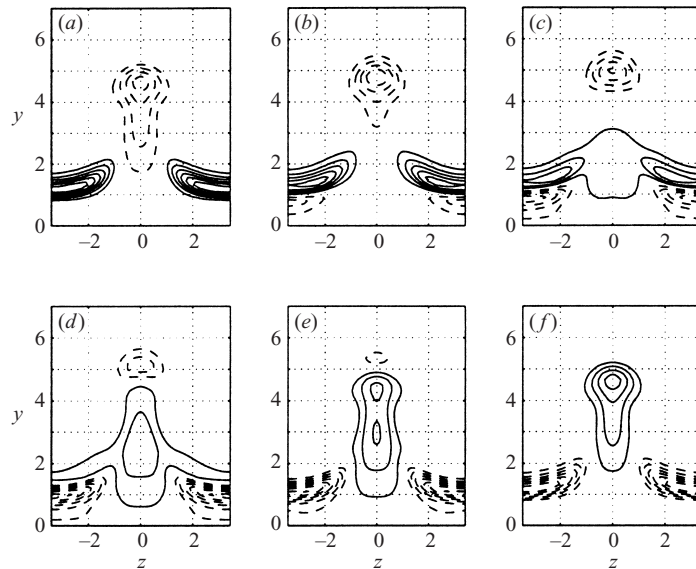
FIGURE 8. Production of streamwise vorticity of the secondary instability mode due to spanwise shear $(\partial U/\partial z)(\partial v/\partial x)$, during half a period of the disturbance evolution at $x = 125$. From time $t = 1\,T/10$ to $t = 6\,T/10$ for (a) to (f). Contour levels: min -6.5×10^{-4}, max 5.5×10^{-4}, spacing 1×10^{-4}.

FIGURE 9. Production of streamwise vorticity of the secondary instability mode due to wall normal shear $-(\partial U/\partial y)(\partial w/\partial x)$, during half a period of the disturbance evolution at $x = 125$. From time $t = 1\,T/10$ to $t = 6\,T/10$ for (a) to (f). Contour levels: min -1.2×10^{-3}, max 1.2×10^{-3}, spacing 2×10^{-4}.

flanks on the low-speed streak. Moreover the w velocity fluctuations are larger than those of v, thus the $-(\partial U/\partial y)(\partial w/\partial x)$ term is the largest one and attains its maximum in the high-speed regions. In fact, one can note that the production of ω_x driven by $\partial U/\partial y$ (figure 9) is located in the regions on top of the low- and high-velocity
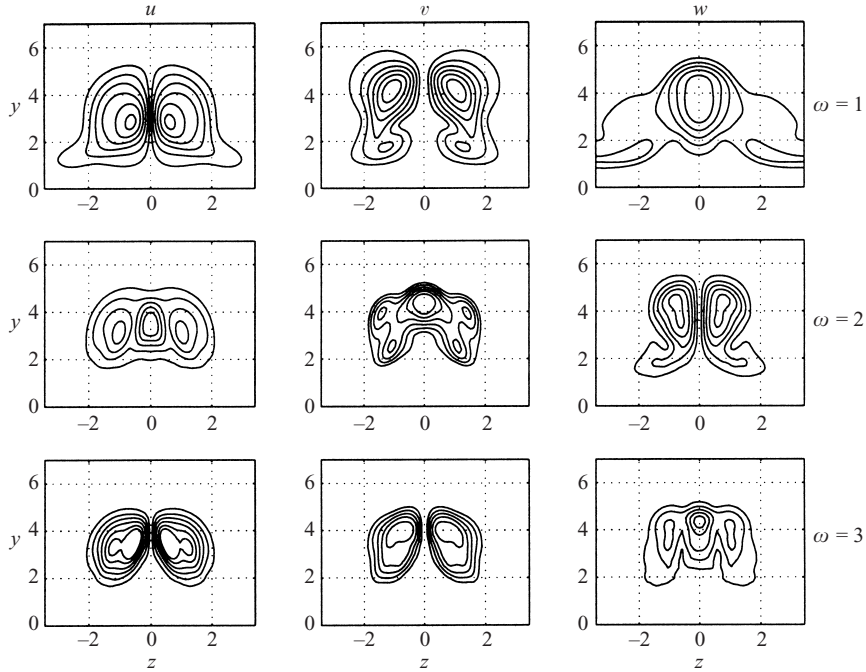
FIGURE 10. Root-mean-square values of the three velocity components in the cross-stream plane at position $x = 175$ at the frequency of the secondary instability mode and its first two harmonics. Contour levels: $u\,(\omega = 1)$ min 2×10^{-3}, max 5.2×10^{-2}, spacing 1×10^{-2}; $v\,(\omega = 1)$ min 3×10^{-3}, max 1.3×10^{-2}, spacing 2×10^{-3}; $w\,(\omega = 1)$ min 8×10^{-3}, max 2.4×10^{-2}, spacing 4×10^{-3}; $u\,(\omega = 2)$ min 2×10^{-3}, max 1.4×10^{-2}, spacing 3×10^{-3}; $v\,(\omega = 2)$ min 1.8×10^{-3}, max 4.3×10^{-3}, spacing 5×10^{-4}; $w\,(\omega = 2)$ min 7×10^{-4}, max 3.9×10^{-3}, spacing 8×10^{-4}; $u\,(\omega = 3)$ min 7×10^{-4}, max 4.5×10^{-3}, spacing 8×10^{-4}; $v\,(\omega = 3)$ min 5×10^{-5}, max 1.7×10^{-4}, spacing 3×10^{-5}; $w\,(\omega = 3)$ min 3×10^{-5}, max 1.5×10^{-4}, spacing 3×10^{-5}.

streaks, while the tilting of ω_z by $\partial U/\partial z$ (figure 8) is responsible for the 'legs' of the ω_x structures observed in figure 6(*d*).

The physical mechanism responsible for streamwise vorticity generation can be explained by considering the eigenmodes of the wall-normal and spanwise velocity, which are both inclined towards the streamwise direction by the mean shear of the base flow. For the first production term in equation (3.1) the inclined v structures directly induce streamwise and spanwise vorticity. This is in turn tilted in the streamwise direction by the mean spanwise shear, leading to the production of new streamwise vorticity. The induced vorticity increases the oscillation of the streak and therefore the wall-normal velocity fluctuations. Thus, the process is self-inducing, with increasing values of the perturbation as it travels downstream. Similarly for the second term on the right-hand side of equation (3.1), the induced streamwise vorticity creates new spanwise velocity and the amplification can continue.

We finally note that the production of the perturbation kinetic energy in the linear stages of the secondary instability is only due to the spanwise shear-driven term, $-(\partial U/\partial z)\,\overline{uw}$.

3.2.3. *Weakly nonlinear stages of transition*

In figure 10 the velocity fluctuation intensities of the fundamental mode and its first two harmonics are shown in a cross-stream plane at position $x = 175$. At this
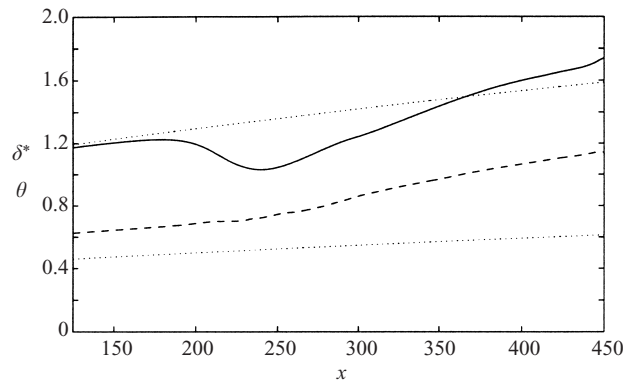
FIGURE 11. Integral boundary layer parameters: ——, displacement thickness δ^*;
- - - -, momentum thickness θ; $\cdots$, theoretical values for laminar Blasius profile.

point nonlinear interaction has begun to be relevant and the higher harmonics are clearly distinguished in the frequency spectra. In the case of sinuous instability the fundamental mode is characterized by fluctuations in the wall-normal and streamwise velocities which are antisymmetric with respect to the line of symmetry of the background streak, while the spanwise velocity is even. Considering that the harmonics are forced by quadratic interactions, it is possible to show that the modes with frequencies 3ω, 5ω, etc. have the same symmetry as the fundamental mode, while for 2ω, 4ω, 6ω, etc. the u, v fluctuations are symmetric and the spanwise antisymmetric. One can also note that the v, w velocity fluctuations are stronger further from the wall than the u component.

3.3. *Time-averaged properties*

We present here the results obtained by averaging the velocity over time, during 50 periods of the fundamental streak instability, and in the spanwise direction. We first show in figure 11 the development of the boundary layer displacement (δ^*) and momentum thickness (θ), together with the theoretical values for a Blasius laminar flow. In the region $200 \lesssim x \lesssim 250$, δ^* decreases, whereas θ is still increasing. The latter is related to the fact that the average skin friction increases. A similar behaviour of the boundary layer thickness and of the momentum loss has been observed by Matsubara & Alfredsson (2001) in a boundary layer subjected to free-stream turbulence. Note also that, at the beginning of the computations, θ is already larger than the laminar value due to the presence of a strong streak.

3.3.1. *Transitional flow*

Mean velocity profiles at various locations in the transitional zone are displayed in figure 12, where the wall-normal coordinate is made non-dimensional with the local displacement thickness δ^*. The evolution from the laminar flow to a turbulent one can be seen. At position $x = 215$ a strong inflectional mean profile is present during the large growth of the skin friction coefficient, see figure 3. In the outer part of the boundary layer one can see an overshoot of the velocity before approaching the final value. The same behaviour of the mean flow was observed by Wu *et al.* (1999) in their simulations of transition induced by free–stream turbulence.

At the early stages of transition, the averaging of the streamwise velocity provides information on the evolution of the streak during the process, since the spanwise modulation dominates in the r.m.s. values. These are displayed in figure 13, together
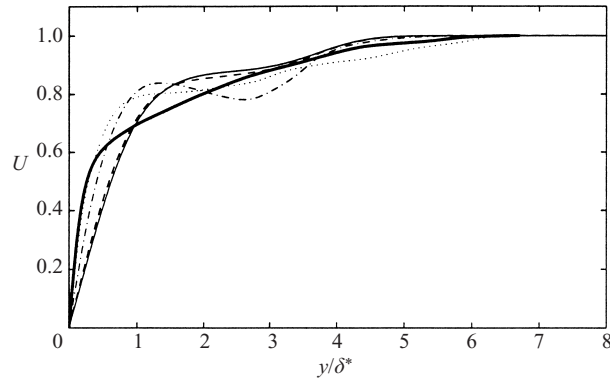
FIGURE 12. Average streamwise velocity in outer coordinates at different streamwise positions:
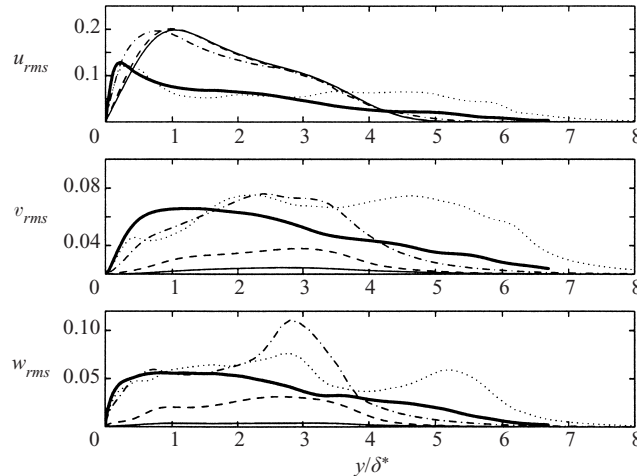——, $x = 126$; ----, $x = 185$; –·–, $x = 215$; ····, $x = 268$; ——, $x = 399$.

FIGURE 13. Root-mean-square values of the three velocity components in outer coordinates at different streamwise positions: ——, $x = 126$; ----, $x = 185$; –·–, $x = 215$; ····, $x = 268$; ——, $x = 399$.

with the other two velocity components. In the experiments of Matsubara & Alfredsson (2001) on transition induced by upstream-generated grid turbulence the u_{rms} value attained by the streaky structure before the breakdown is about 11–12%. In our case, instead, the streak amplitude at the beginning of transition is about 19%, but, as observed in Wundrow & Goldstein (2001), the averaged values usually reported in the experiments are likely to mask the stronger localized distortions which induce the breakdown. However, the same qualitative behaviour of u_{rms} is observed as in the experiments, i.e. the peak is sharpening, moving closer to the wall and reaching values of approximately 12–13%.

As the flow develops downstream, the r.m.s. values of the wall-normal and spanwise velocity components increase, especially in the outer part of the boundary layer, around $y \approx 3$. This corresponds to the wall-normal region where the secondary instability is localized, see figure 10. One can also note that the spanwise velocity fluctuations are larger than the wall-normal ones, and a considerable value of $w_{rms} \approx$ 11% is attained at $x = 215$. This result is not unexpected since the kind of instability
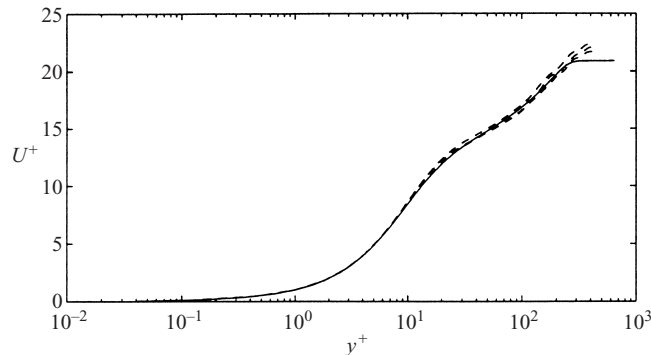
FIGURE 14. Mean streamwise velocity profiles in inner scaling: - - - -, present simulations at $Re_\theta = 845$ ($x = 360$), $Re_\theta = 875$ ($x = 375$) and $Re_\theta = 910$ ($x = 400$); ——, Skote (2001) simulations at $Re_\theta = 685$.

studied is characterized until its late stages by strong spanwise oscillations of the low-speed streak. It is also interesting to notice that at $x = 268$ the mean velocity profile, figure 12, and u_{rms} are very close to the turbulent ones, especially close to the wall, but v_{rms} and w_{rms} are characterized by large values in the upper part of the boundary layer. As we will see in a later section, these oscillations represent structures formed in the transition region which survive downstream while the shear stress at the wall increases and the near-wall flow may be considered turbulent.

3.3.2. *Quasi-turbulent flow*

In this section we discuss the results of the statistics obtained towards the downstream end of the simulations, where the flow becomes uncorrelated to the inflow conditions and the skin friction coefficient approaches turbulent values, see figures 3 and 4.

The mean velocity profiles are displayed in inner coordinates in figure 14 at three different downstream positions, together with the results from the spatial simulations of a fully turbulent boundary layer with zero pressure gradient by Skote (2001) are shown for comparison, although for a lower value of the momentum thickness Reynolds number Re_θ. Profiles of the time-averaged turbulence kinetic energy production normalized with wall parameters are shown in figure 15 at the same three streamwise stations and compared again with the DNS data of Skote (2001). Note that all profiles show a maximum of $P^+ = 0.25$ at $y^+ = 12$, showing self-similarity.

The r.m.s. values for the three velocity components are displayed in figure 16. The results show large differences compared to a fully turbulent flow in the outer part of the boundary layer, where periodic flow structure are still present, as shown earlier. Thus, analysis of the results indicates that the averaged quantities reproduce well close to the wall the features of a turbulent flow.

3.4. *Flow structures*

3.4.1. *Overall features*

Before discussing in detail the instantaneous flow structures we first give a general idea of the transition scenario by showing snapshots of the flow. In figure 17 the instantaneous streamwise velocity component of the perturbation is shown in a longitudinal plane perpendicular to the wall for $z = 0$, corresponding to the centre of the undisturbed low-speed streak, and in a plane parallel to the wall, at $y = 0.47$. The
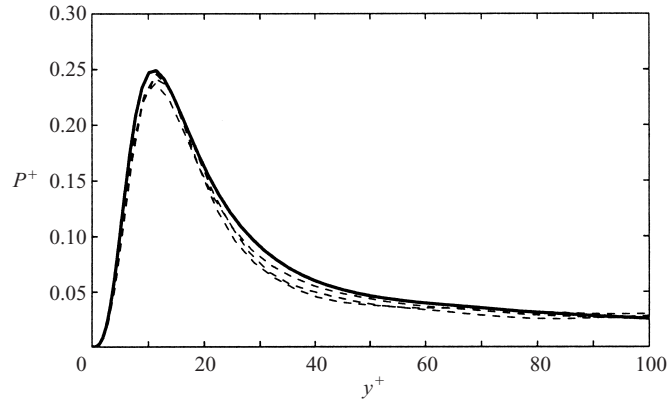
FIGURE 15. Time-averaged non-dimensional turbulence kinetic energy production, $P^+ = -\overline{uv}^+ \partial U^+/\partial y^+$, near the wall: ----, present simulations at $Re_\theta = 845$ ($x = 360$), $Re_\theta = 875$ ($x = 375$) and $Re_\theta = 910$ ($x = 400$); ——, Skote (2001) simulations at $Re_\theta = 685$.
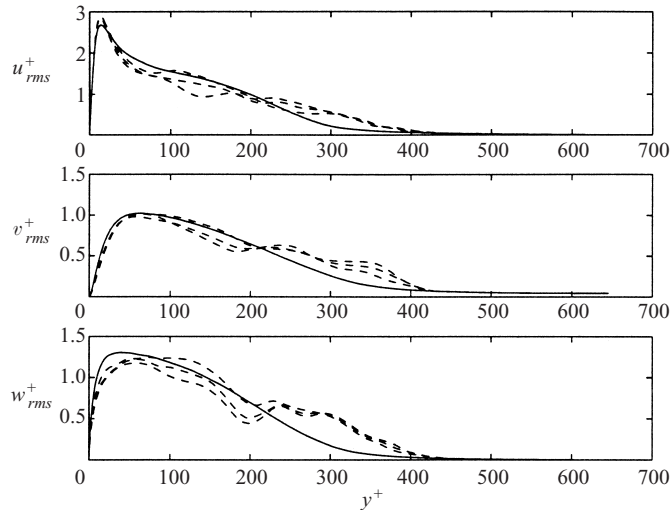

FIGURE 16. Root-mean-square values of the three velocity components in inner coordinates: ----, present simulations at $Re_\theta = 845$ ($x = 360$), $Re_\theta = 875$ ($x = 375$) and $Re_\theta = 910$ ($x = 400$); ——, Skote (2001) simulations at $Re_\theta = 685$.

perturbation velocity field is defined as the difference between the solution velocity field and the mean value in the spanwise direction for each value of x and y. It can be clearly seen that the sinuous instability consists of harmonic antisymmetric streamwise oscillations of the low-speed region. In figure 17(*a*) one can note that the perturbation is first seen in the outer part of the boundary layer. The disturbance then moves towards the wall until the wall shear is considerably increased. At the end of the computational box some periodicity can still be seen in the disturbance in the outer part of the boundary layer, as discussed previously, while close to the wall the flow is now turbulent. In figure 17(*b*) two streaks can be seen within one computational domain at the end of the transition process; note that the spanwise dimension of the box for $x > 350$ is less than 275 in wall units.

A three-dimensional picture of the flow field from the laminar to the turbulent region is shown in figure 18. The lighter grey isosurface represents the low-speed
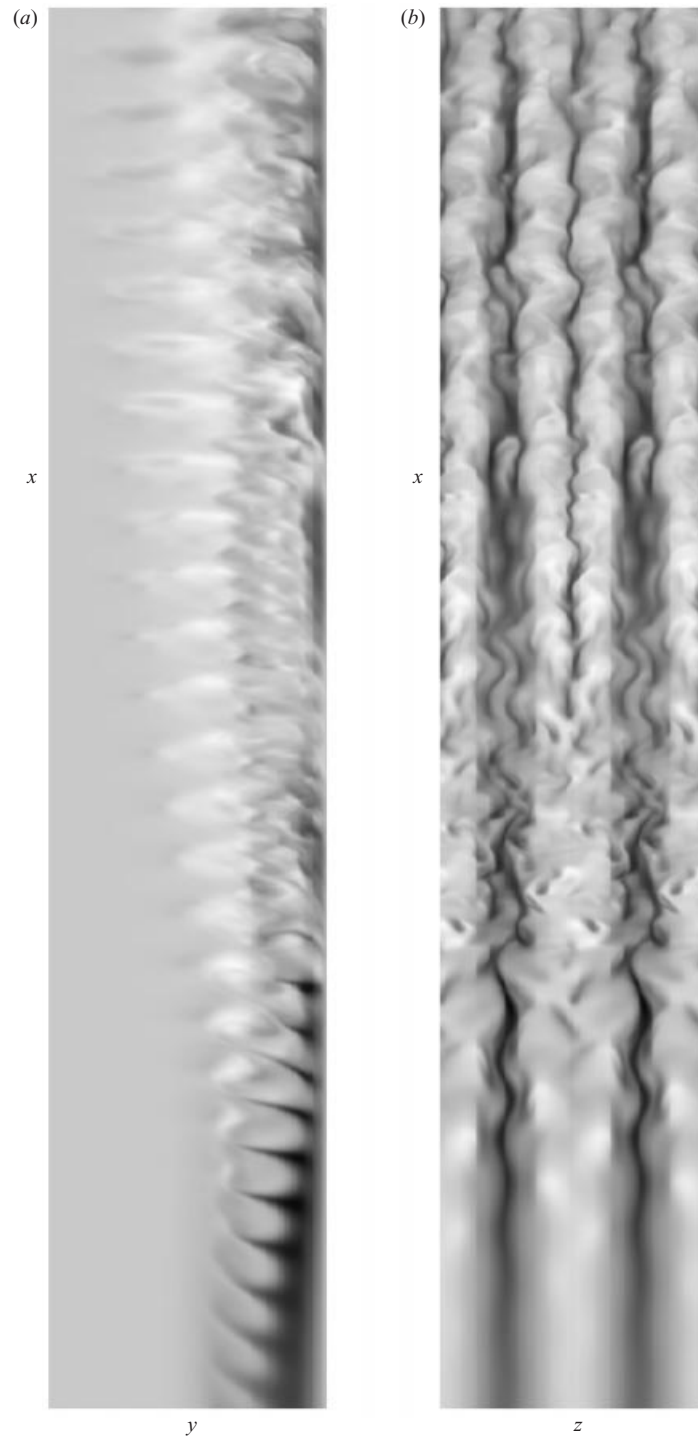
FIGURE 17. Visualization of streak breakdown using the streamwise velocity component of the perturbation in (*a*) a wall-normal (x, y)-plane at $z = 0$ and (*b*) a wall-parallel (x, z)-plane at $y = 0.45$. $x \in [185, 360]$. Grey scale from dark to light corresponds to negative to positive values. The flow is from bottom to top. In (*b*) two spanwise streaks are displayed.
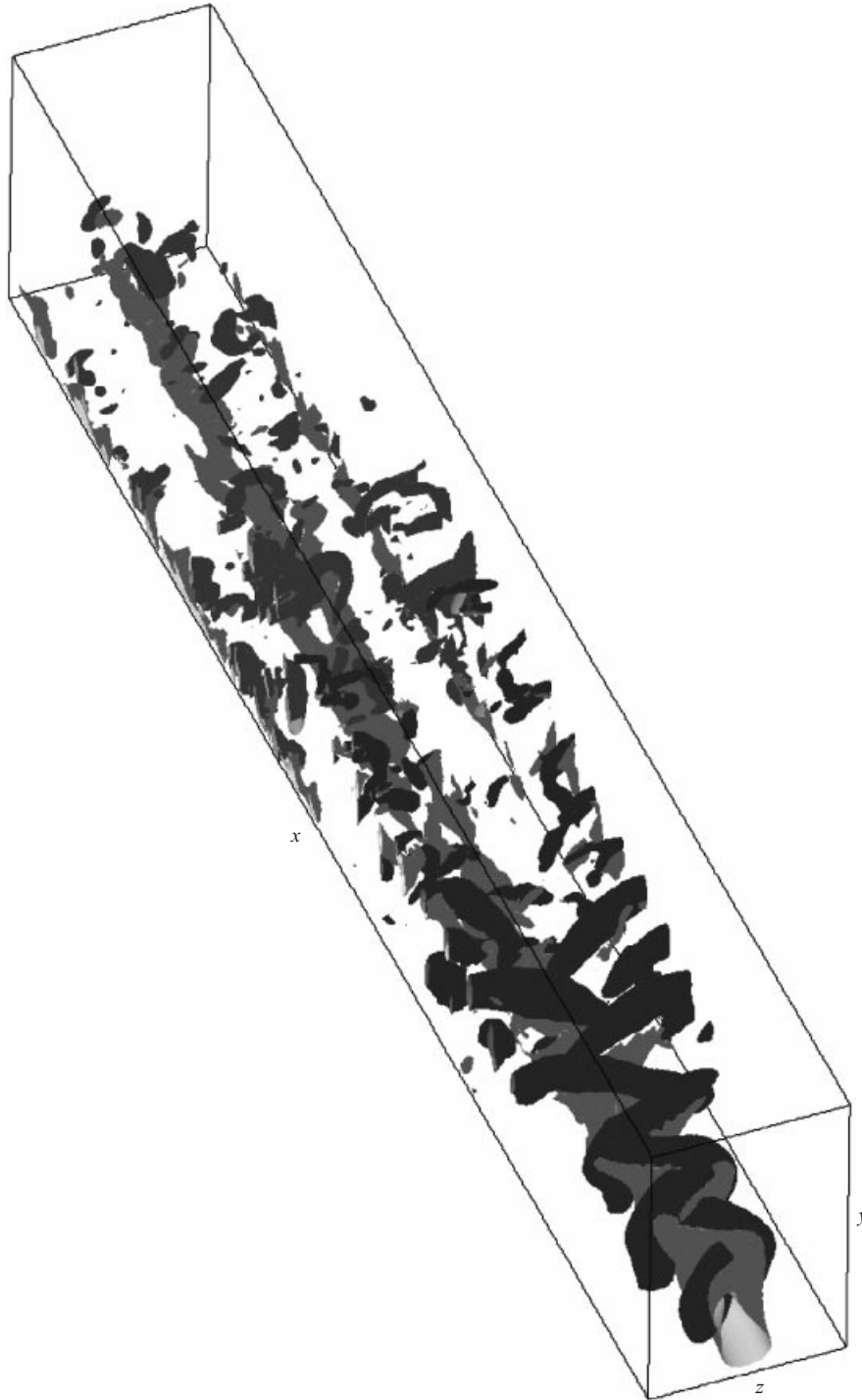
FIGURE 18. The flow field from the laminar to the turbulent region. The x-values correspond to the range $x \in [185, 360]$. The grey structures are the low-speed streaks and the darker ones are regions with low pressure. Contour levels are -0.14 for the streamwise velocity fluctuations and -0.014 for the pressure for $x < 268$ and -0.0065 further downstream. The streamwise scale is one third of the cross-stream scale.

streaks, while the dark grey represents regions of low pressure. These correspond to strong rotational fluid motions and are used to identify vortices. Also, visualizations using negative values of the second largest eigenvalue of the Hessian of the pressure (see Jeong *et al.* 1997) are performed and no relevant differences are observed. The main structures observed during the transition process consist of elongated quasi-streamwise vortices located on the flanks of the low-speed streak. Vortices of alternating sign are overlapping in the streamwise direction in a staggered pattern and they are symmetric counterparts, both inclined away from the wall and tilted in the downstream direction towards the middle of the undisturbed low-speed region. The strength and extent of these vortices and the spanwise motion of the low-speed streak increase downstream before the breakdown. Note also that the downstream end of the streamwise vortices, located in the outer part of the boundary layer, is tilted and propagates in the spanwise direction to form arch vortices. Towards the end of the box the flow has a more turbulent nature and more complicated low-pressure structures occur. It also seems that there is no connection between the laminar and turbulent region low-speed streaks, since the streak is disrupted at transition and those which appear downstream are not a continuation from upstream.

3.4.2. *Late stages of transition*

To study in detail the late stages of the streak breakdown, we plot in figure 19 the instantaneous flow in vertical planes at different streamwise positions, covering a distance corresponding to about one half of the secondary instability wavelength. The velocity vectors show the spanwise and wall-normal velocity. The thick black isolines represent the streamwise velocity and the white line regions of low pressure. In the background, the streamwise vorticity is shown from negative values (light areas) to positive (dark areas). One can follow the evolution of one of the two quasi-streamwise vortices observed in figure 18, namely the one characterized by negative vorticity, located on the flank of the low-speed streak denoted by negative z. In figure 19(a) one can note that the vortex with $\omega_x > 0$ is still visible in the upper part of the boundary layer, where the pressure attains its minimum value. However a negative vortex, i.e. with rotation in the counter-clockwise sense, is already formed below this and is moving in the positive z-direction and towards the upper part of the boundary layer. Regions of strong negative streamwise vorticity are associated with vortices; positive values of ω_x indicate instead regions of strong spanwise gradient of the wall-normal velocity on the positive flank of the low-speed streak and region of wall-normal gradient of the spanwise velocity in the dark area above the high-speed streak. Similarly when the streak is moving in the negative z-direction, regions of positive ω_x are associated with vortices. By symmetry, the ω_x distribution half a wavelength away is obtained by reflection and sign inversion (apart from the amplification downstream). Comparing the areas of negative streamwise vorticity of the full velocity field with the isosurfaces of the same quantity displayed in figure 6(d), one can note that only one of the two legs observed in the secondary instability mode is still present as the main feature of the breakdown. We note also that the leg which is able to induce stronger streaks and then to create stronger mean shear is the one which is still amplified and survive in the late stages. Its symmetric counterpart is working to reduce the mean flow modulation and so it is reasonable to assume that this is the reason for its disappearance. Analysis of the first harmonic of the secondary instability mode shows in fact that the phase lock between the two is such that negative ω_x is increased for negative z. The odd symmetry of this mode implies that at the same time positive ω_x is balancing the negative leg located on the
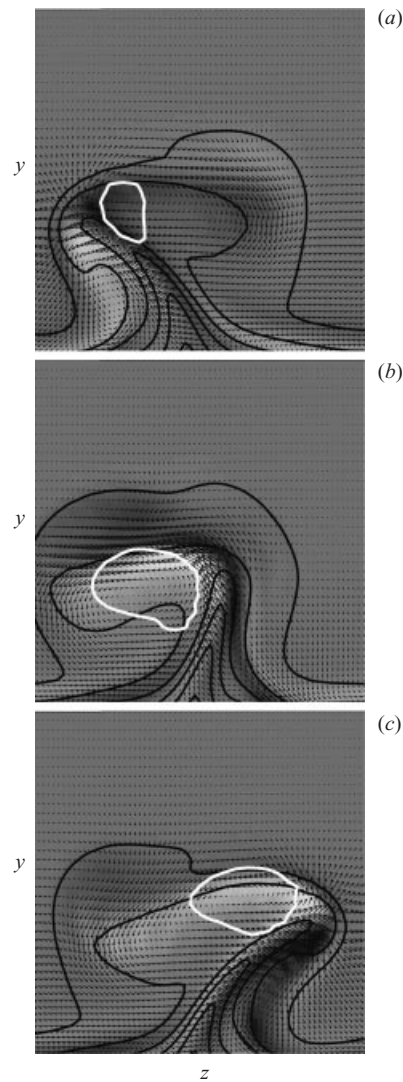
FIGURE 19. Vertical cross-stream planes at positions (*a*) $x = 208$, (*b*) $x = 211$, (*c*) $x = 213$. The velocity vectors represent spanwise and wall-normal velocity. Thick black isolines represent the streamwise velocity and the white line regions of low pressure. The background shows values of streamwise vorticity from negative values (light areas) to positive (dark areas).

positive side of the low-speed streak. The first harmonic of the secondary instability mode acts also to induce negative vorticity ahead of the V structure typical of the fundamental mode, as can be observed in figure 19(*c*) where the negative vortex has reached regions of positive z.

Following the evolution of the streamwise vorticity from the linear amplification to the late stages, we note that at the early stages, the instability growth is characterized by increasing values of the flattened ω_x structures displayed in figure 6(*d*), with the spanwise symmetry of the eigenfunction slightly destroyed by the higher harmonic and by the mean streamwise vorticity. At downstream position $x \approx 205$ the negative and positive ω_x structures are located on the negative and positive flanks of the

low-speed region and follow its oscillations (see figure 19). Note also that the low-speed streak is becoming narrower. The final stages of the breakdown are shown in figure 20, in plots similar to the ones of figure 19. In figure 20(a) one can see that as the oscillation of the low-speed region is increased, the upper part of it is subjected to strong motion in the negative direction while the lower part has begun to move in the opposite direction. A similar phase delay between the top and bottom parts of the streak during the sinuous breakdown was also observed in channel flow by Elofsson *et al.* (1999). Considering the dark and light areas in figure 20(a), one can note that the adjacent layers of positive and negative ω_x, located in the low-speed region, roll up to form an arc in the (y, z)-plane. As a result of this the upper part separates and continues its periodic motion in the outer part of the boundary layer. This can be seen in figure 20(b) where one can also note that the low-speed region is now localized closer to the wall. This lower streak is still subjected to sinuous instability and two vortices can be seen: a positive one similar to the ones observed in figure 19, located on the flank of the streak, and a negative one further away from the wall as a trace of the previous oscillation in the opposite direction. The region of large ω_x on the flank of the streak in figure 20 now appears much more localized. The breakdown of the lower streak is then similar to the process already observed. The higher and lower parts are moving in opposite directions and the streak is disrupted. Finally, figure 20(c) shows an instantaneous plot of the flow downstream of the breakdown, where many and disordered structures can be observed.

In figure 21 we display at the actual scale a view from the top of isosurfaces of positive and negative wall-normal vorticity, ω_y, in the final stages of the breakdown. This quantity is almost entirely determined by the mean spanwise shear, $\partial U/\partial z$, so that its downstream evolution is dominated by the spanwise motion of the low-speed region. It is interesting to notice how the upper part separates and continues its motion independently (see the tongue-like structures on the sides of the central low-speed streak). We recall that structures of spanwise vorticity in a plane normal to the wall at $z = 0$ are shown in figure 1. In this case it is the mean normal shear, $\partial U/\partial y$, which determines the largest vorticity. The thin periodic structures represent the shear induced by the motion of the low-speed streak. From this, we can conclude that, except for the arch vortices displaced in the outer part of the boundary layer, the structures of ω_y and ω_z are determined by the motion of the low-speed streak and its associated strong shear layers.

Finally we analyse in detail the main structures detected at the late stages of the transition process. In figure 22 we display a top and side view, at the actual scale, of the low-pressure structures shown before. The region of instantaneous negative streamwise velocity perturbation is also shown for reference. From the top view one can note how the vortices form arches in the spanwise direction invading the whole domain. The side view shows quasi-streamwise structures, tilted away from the wall, which look similar to the leg of the Λ-vortex observed in transition initiated by TS-waves, see Rist & Fasel (1995) for example. However, the top view clearly reveals the staggered pattern of these structures. Figure 23 shows the flow pattern in a smaller region, of streamwise extent equal to about one wavelength of the secondary instability mode, just before the final breakdown. The low-speed region is now lower than the original laminar unstable streak. It is still oscillating in the spanwise direction and there are quasi-streamwise vortices located on its flanks in a staggered pattern. In the outer part of the boundary layer, the arch vortices formed before can be seen. They are now uncorrelated to the streak oscillation underneath.
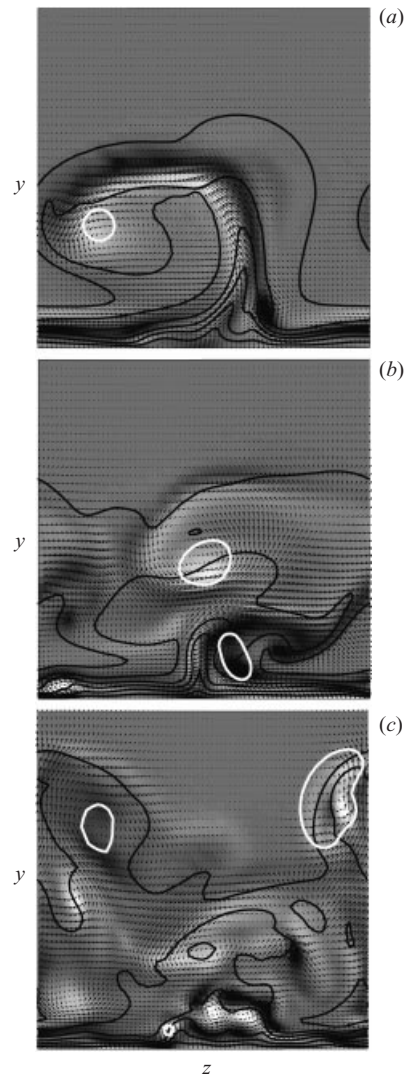
FIGURE 20. As figure 19 but at positions (*a*) $x = 221$, (*b*) $x = 234$, (*c*) $x = 256$.
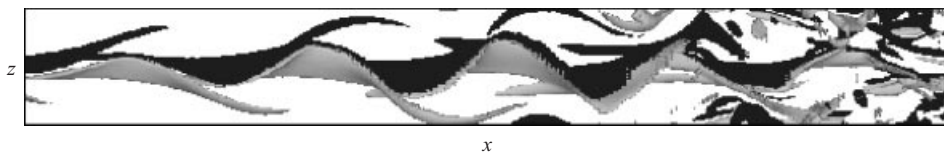

FIGURE 21. Top view of isosurfaces of positive (lighter grey) and negative (dark grey) wall-normal vorticity, $\omega_y = \pm 0.53$. $x \in [190, 245]$.

3.4.3. *Visualization by timelines*

In experimental investigations of boundary layer transition flow structures are typically investigated through flow visualizations using either hydrogen bubbles or smoke. Here we perform a numerical visualization following the evolution of massless particles. Timelines are generated by releasing particles along lines parallel to the spanwise
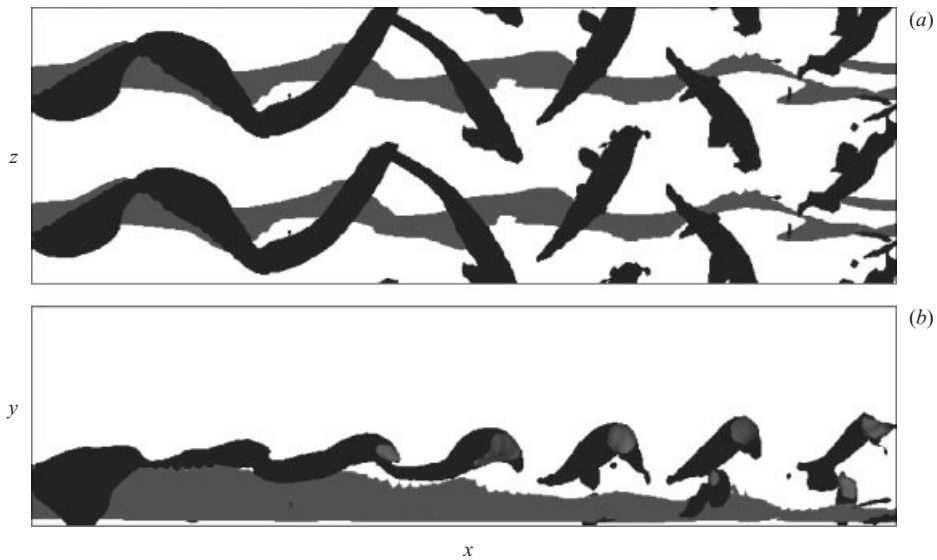
FIGURE 22. (*a*) Top and (*b*) side view of the structures at the late stages of transition. $x \in [203, 245]$. Lighter grey represents negative streamwise velocity perturbation and dark grey regions of low pressure. In (*a*) two spanwise streaks are displayed.
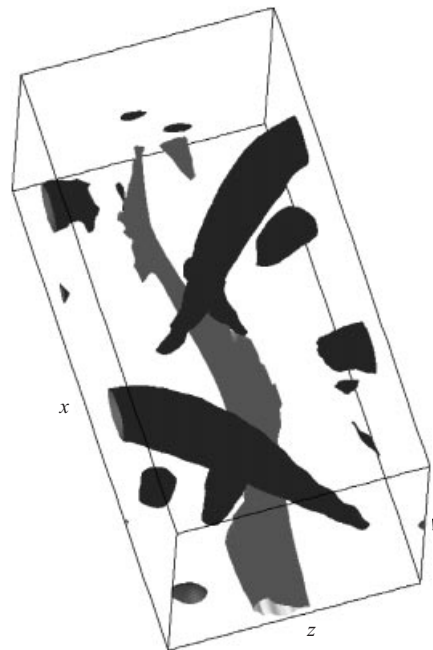

FIGURE 23. Structures at the late stages of transition, shown for one wavelength of the secondary instability. $x \in [227, 239]$. Grey represents negative streamwise velocity perturbation and dark grey regions of low pressure. The flow is from the bottom to the top.

direction at different times during one period of the secondary instability mode. The instantaneous evolution of these particles is determined by the instantaneous velocity field. In figure 24 we display the evolution of a single material line released at position $x = 150$ and $y = 3$. Two streamwise vortical structures can be seen on the sides of
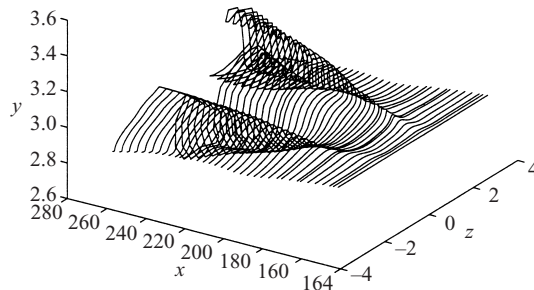
FIGURE 24. Evolution of a spanwise material line released at position $x = 150$ and $y = 3$.

the low-speed region; one is growing and moving away from the wall while the other is approaching the wall. The structures observed from the evolution of a line released half a period later would present the opposite behaviour. Since the particles followed are located in the outer part of the boundary layer, a regular pattern can also be seen downstream of the transition point, $x \approx 250$. Note that the smoke visualizations by Asai *et al.* (1999) in a cross-stream plane also show the presence of vortical structures on the flanks of the low-speed streak. The evolution of a material line normal to the wall released at the centre of the low-speed streak has also been studied. The motion of the particles consists of spanwise oscillations of different amplitude and phase at different distances from the wall.

4. Discussion

4.1. *Relation to transition induced by free-stream turbulence*

Experiments on boundary layers subject to free-stream turbulence show that transition is characterized by the occurrence of strong streamwise streaks (Klebanoff 1971; Kendall 1985; Westin *et al.* 1994). In Andersson *et al.* (2001) and Matsubara & Alfredsson (2001) it was also shown that the wall-normal mode shape of the optimal disturbance found in the theoretical works of Andersson *et al.* (1999) and Luchini (2000) are remarkably similar to the u_{rms} values measured in boundary layers with free-stream turbulence. A nonlinear mechanism for boundary layer receptivity to free-stream disturbance has been proposed by Berlin & Henningson (1999) and Brandt, Henningson & Ponziani (2002); this is responsible for the generation of streamwise vortices, which in turn induce the growth of similar streaks. It is now understood that the growth of streaks can be explained successfully by the theory of non-modal growth. However, there is still uncertainty in the way turbulent spots are formed in the boundary layer, once strong streaks are present. In fact, controlled experiments are impossible in a boundary layer under free-stream turbulence and no definitive proof is given of a secondary instability. Flow visualizations (Matsubara & Alfredsson 2001) show that some streaks develop a streamwise waviness of relatively short wavelength, before the formation of spots. These authors attribute this wavy type of motion to a secondary instability, leading to laminar–turbulent transition analogously to what has been observed in channel flows (Reddy *et al.* 1998; Elofsson *et al.* 1999) and in boundary layer flows under controlled conditions (Bakchinov *et al.* 1995; Asai *et al.* 1999). In the theoretical work of Wundrow & Goldstein (2001) it is shown how initially linear, but of broadband nature, perturbations of the upstream flow ultimately lead to strong shear layers in certain localized spanwise regions. These

highly inflectional shear layers can then support rapidly growing inviscid instabilities. Jacobs & Durbin (2001) write that no evidence of sinuous, or other prefatory streak instability, is observed in their simulations of a boundary layer under free-stream turbulence. Jacobs & Durbin (2001) conjecture that streaks become a receptivity site for smaller-scale free-stream turbulence which initiates an instability near the top of the boundary layer.

In the present work we use a simpler flow configuration (steady streak) and show that sinuous instability can lead directly to a turbulent flow and that some of the basic averaged flow data present interesting similarities with experiments and/or simulations of by-pass transition under free-stream turbulence. An important similarity is observed in the development of the boundary layer thickness. The peculiar decrease of this parameter during the late stages of transition seems to be a common feature of our simulation and the experimental results of Matsubara & Alfredsson (2001), which was not observed in other transition scenarios. Future experiments and numerical simulations may be compared with the present results in order to assess a firmer connection between the proposed transition scenario and the streak breakdown in boundary layers subjected to free-stream turbulence. For this purpose it is important to re-emphasize that in order to isolate and observe the features of the streak transition scenario we have simulated the spatial evolution of an instability mode which is induced by a continuous harmonic forcing at the upstream inlet. In a boundary layer subject to free-stream turbulence the secondary instability would, rather, be triggered by localized perturbations, more likely the ones present in the free stream. Therefore the instability would then develop as a localized wavepacket.

4.2. *Comparison to O-type, K-type and H-type transition*

In this section, we compare the late stages of transition initiated by sinuous instability of streamwise streaks with three different scenarios, observed and studied in flat-plate boundary layers. We consider transition initiated by a pair of oblique waves (O-type), and K- and H-type transition, resulting from the secondary instability of TS-waves. The reader is referred to the experimental study of Bake, Fernholz & Kachanov (2000) for a recent thorough investigation of the resemblance of K- and H-regimes.

Berlin *et al.* (1999) noticed that the structures they identified in the late stages of oblique transition have many similarities with those previous investigations have found in the K- and H-type transition. In fact, they observed that before the flow has reached a fully turbulent state, Λ-shaped structures, consisting of pairs of streamwise counter-rotating vortices are formed. They also noted that inside the Λ-structures there is an upward motion. The lift-up of low streamwise velocity causes strong wall-normal gradients, located on top of the Λ-vortices, again in close similarity to the shear layers observed by Williams, Fasel & Hama (1984) and Rist & Fasel (1995) for example, in K-type transition. Measurements using hot-wire probes revealed that the positions of the Λ-shaped vortices coincided with the appearance of u_{rms} peaks and high-frequency oscillations (spikes). Further, the Λ-vortices observed in O-type transition are associated with inflectional profiles in both the normal and spanwise directions. Berlin *et al.* (1999) explained the similarities between the O-, K- and H-regimes by considering the common features of all three transition scenarios, namely oblique waves and streamwise streaks. They speculated that the pattern of Λ-vortices appearing in these three transition scenarios is independent of the presence of Tollmien–Schlichting waves. Using a criterion of positive interference of the normal

velocity between the streamwise vortices and the oblique waves, they were able to predict the appearance of the Λ-vortices.

In the present case, streamwise streaks and oblique waves are also the fundamental features at the breakdown and the structures observed present similarities and differences. Similarly to the other transition scenarios, we have found counter-rotating streamwise vortices located on opposite flanks of the low-speed region; the vortex with $\omega_x > 0$ being on the positive side. The structures are inclined away from the wall and tilted in the downstream direction towards the middle of the undisturbed low-speed region. However, the streamwise vortices appear in a staggered pattern, alternating in the streamwise direction. Comparing the present case with oblique transition, we note that the different alignment of the streamwise vortices is due to the symmetry of the fundamental perturbation growing on the streaks. Analysis of the results presented in Berlin *et al.* (1999), shows in fact that the strong streaks induced by nonlinear interactions are perturbed by periodic disturbances, given by the oblique waves themselves, which are symmetric with respect to the streak. Looking also at the symmetry of the late stages of the breakdown, we can relate oblique transition to varicose instability of the streaks.

The different symmetry of the streamwise vorticity perturbation can be used to explain similarities and differences observed in the two scenarios. In the present work, we have followed the evolution of the streamwise vorticity and noted that the initially symmetric distribution is disrupted towards the breakdown. Of the two symmetric 'legs' of positive and negative ω_x alternating in the streamwise direction which can be seen in an instantaneous configuration, only one is amplified downstream, specifically the leg which is able to induce stronger shear layers on the mean flow. Thus, we recover the staggered pattern of quasi-streamwise vortices observed at the final stages of the breakdown. In Berlin *et al.* (1999), isosurfaces of positive and negative instantaneous streamwise vorticity are also shown. One can note that the distribution of ω_x is now antisymmetric. The downstream evolution of ω_x is also characterized by the growth of structures with positive sign on the positive side of the low-speed streak and with negative sign on the negative flank. In this case, however, the structures are not staggered in the streamwise direction and they appear with the typical Λ-shape. The same ideas apply in K- and H-type transition, where the oblique modes of the perturbation are also symmetric with respect to the streamwise vortices. We also note that the same interference criterion introduced in Berlin *et al.* (1999) can be used in the present transition scenario. Interference of positive wall-normal velocity of the secondary instability mode and of the mean flow can lead to the appearance of a single streamwise vortex on a side of the low-speed region.

The four transition scenarios considered show different behaviours at the downstream tip of the quasi-streamwise vortices. In transition induced by TS-wave instability, a spanwise vortex connecting the legs of the Λ-vortex is observed. This is due to the fact that strong spanwise vorticity is already present as it characterizes the primary instability. Two-dimensional Tollmien–Schlichting waves consist in fact of rolls of spanwise vorticity concentrated around the critical layer. The secondary instability induces a three-dimensional flow and hence streamwise vorticity, by bending the ω_z structures (see Herbert 1988). In oblique transition instead, the legs of the Λ-structures develop independently and are then drawn towards each other. The same evolution of the streamwise vortices is observed in the present case; however the lack of a symmetric counterpart on the other side of the low-speed streak allows the vortex to tilt, cross the low-speed region and generate the observed arches.

4.3. *Comparison to transition in vortex-dominated flows*

The secondary instability mechanisms considered here show similarities with transition in flows with curvature or in rotating channels, where the dominating instability results in streamwise vortices which, in turn, create streaks (see Swearingen & Blackwelder 1987; Li & Malik 1995, for the case of Görtler vortices). Further, three-dimensional vortical structure detected in the simulations of transition to turbulence in Görtler flow performed by Liu & Domaradzki (1993) show interesting analogies with transition in Blasius flow. In fact, they observed that close to the transition point vorticity structures are associated with a series of connected hairpin vortices in the outer part of the boundary layer. However, these vortices play a smaller role in the transition process than the streamwise vortical structure which is observed to develop close to the wall in the low-speed region between the vortices. They note, in fact, that the turbulent kinetic energy production is related to regions of large spanwise shear. This high-vorticity structure is associated with the sinuous mode of the secondary instability. Park & Huerre (1995) studied the secondary instability of Görtler vortices and found that the sinuous mode completely dominates close to the wall, while the varicose mode is strong near the head of the low-speed region. They indicate, in agreement with Liu & Domaradzki (1993), that the sinuous mode is dominant in the transition and that the horseshoe vortices observed can be interpreted as arising from the nonlinear evolution of the varicose mode (also unstable but with lower growth rates). We recall here that the streaks considered in the present study are unstable only to antisymmetric disturbances and therefore a simpler scenario is expected as the disturbance reaches such high levels that it disrupts any type of flow symmetry. It is interesting to note also that Liu & Domaradzki (1993) documented the formation in the turbulent regime of two low-speed streaks located close to the wall in the region of the original low- and high-speed streaks; this is very similar to what we observed in the present simulation towards the end of the computational box.

4.4. *Comparison to streak instabilities in the near-wall region of turbulent flows*

Streamwise vortices and streaks are also fundamental structures in the near-wall region of turbulent boundary layers and the vortices seem to be related to streak instabilities. In fact, the structures we identified show a close resemblance to the ones detected in turbulent wall flows (see Schoppa & Hussian 1997; Jiménez & Simens 2001). Kim, Kline & Reynolds (1971) were the first to show the importance of local intermittent inflectional instability in the bursting events, which are associated with periods of strong turbulent production. They observed three oscillatory types of motion of the streaks: a growing streamwise vortex, a transverse vortex and a wavy motion in the spanwise and wall-normal directions. Later, Swearingen & Blackwelder (1987) compared and related the latter two modes observed in Kim *et al.* (1971) to the secondary varicose and sinuous instability of streamwise vortices measured during transition on a concave wall. In the same way as Swearingen & Blackwelder (1987), we can speculate that the first type of oscillatory motion observed by Kim *et al.* (1971), i.e. growth of a streamwise vortex, which is by far the most often observed in their experiments, is related to the growth of either of the two streamwise vortices observed on the flank of the low-speed streak. This is a common feature of sinuous and varicose instability, see the discussion in the previous section, and therefore it is the most likely to be visualized if the hydrogen bubbles are released slightly off-centre of the low-speed streak. Recent studies on the instability of a base flow generated by the superposition of a turbulent mean flow and the streaky structures (Waleffe 1997; Schoppa & Hussain 1997; Kawahara *et al.* 1998) have found that the dominating

instability is sinuous. In fact, the evolution of the streamwise vorticity observed in the present simulations of transitional flow is similar to that observed by Schoppa & Hussain (1997) in their analysis of the streak instability in the near-wall region of a turbulent flow. Schoppa & Hussain (1997) attribute the formation (collapse) of regions of strong vorticity with compact cross-section, similar to the one observed in figure 20(*b*), to the local vortex stretching due to positive $\partial u/\partial x$. The strong spanwise shear of the flow is responsible for the generation of $\partial u/\partial x$ as the oscillation of the low-speed region reaches considerable amplitudes. Regions of positive $\partial u/\partial x$ are located downstream of the streak crests, causing direct stretching of the local ω_x. Note also that the behaviour of the region close to the wall from the final stages of the transition is similar to that observed by Jiménez & Pinelli (1999) and Jiménez & Simens (2001) in limiting conditions for the streak cycle to be self-sustained (see as example the structures close to the wall in figure 23).

On the other hand, in the experiments by Acarlar & Smith (1987) a low-speed streak was generated in an otherwise laminar boundary layer by blowing through a slot in the wall. The streak became unstable and horseshoe vortices were formed. In the simulations by Skote, Haritonidis & Henningson (2002) the Acarlar & Smith (1987) experiment was numerically reproduced and the process of horseshoe vortex generation further investigated. Skote *et al.* (2002) show that the appearance of an unstable wall-normal velocity profile is a precursor to the appearance of horseshoe vortices, and thus associated to varicose instability of the turbulent streaks. We note that 'streamwise vortices staggered' on both the flanks of the low-speed streak and hairpin vortices have been observed in turbulent boundary layers. We, therefore, believe that both types of streak instability are present in turbulent boundary layers and that the mechanisms and scenarios observed in the transition of streaky structure are closely related to the near-wall events in turbulent flows, in spite of the different time and space scales involved.

5. Summary and conclusions

We have performed the first numerical simulation of a by-pass transition scenario initiated by the sinuous instability of a streamwise streak in an incompressible flat-plate boundary layer flow. Andersson *et al.* (1999) and Luchini (2000) showed that the perturbations at the leading edge of a flat plate that show the highest potential for transient energy amplification consist of a pair of streamwise vortices. Due to the lift-up mechanism these optimal disturbances lead to elongated streamwise streaks downstream. If the streak amplitude reaches a threshold value, secondary instability can occur and provoke transition. The most dangerous type of secondary instability has been found by Andersson *et al.* (2001) to be the sinuous one, consisting of spanwise oscillation of the low-speed region. Here, we have studied in detail the late stages of transition originating from this scenario and compared them with other transition scenarios and flows where streak instability is also present. The following points summarize the main findings.

The main structures observed during the transition process consist of elongated quasi-streamwise vortices located on the flanks of the low-speed streak. Vortices of alternating sign are overlapping in the streamwise direction in a staggered pattern, both inclined away from the wall and tilted in the downstream direction towards the middle of the undisturbed low-speed region.

We have followed the evolution of the streamwise vorticity of the perturbation. The streamwise vorticity of the secondary instability mode is symmetric with respect to the streak; structures of the same sign appear above the low- and high-speed

streak, connected by legs situated along the flanks of the low-speed region. Positive and negative structures alternate in the streamwise direction. At the late stages of the breakdown only one of the two legs is still present and amplified. This is the leg which is able to induce stronger streaks and in turn to create stronger mean shear. The observed staggered pattern is a result of this process.

At the late stages, we observe an increasing phase difference between the lower and upper parts of the low-speed streak, which are then moving in opposite directions. Thus the streak is disrupted. The periodic motion of the upper part continues far downstream in the outer part of the boundary layer, while closer to the wall streaks of turbulent nature are observed.

In other transition scenarios (see Rist & Fasel 1995; Berlin *et al.* 1999, for numerical studies on the late stages), positive and negative streamwise vortices are also present on the side of the low-speed region but they are not staggered in the streamwise direction. Instead the left and the right streamwise vortices join at the centre of the streak and form the typical Λ-structures seen in K- and H-type transition. The difference is found in the symmetry of the streamwise vorticity of the fundamental secondary instability. In the present case the vorticity disturbance is symmetric, while in oblique transition and K- and H-type of transition the streamwise vorticity is antisymmetric. A common feature of the scenarios considered, is that the vortex which is amplified at the late stages is the one which is inducing a stronger mean shear.

The structures and their evolution observed in the present simulation of a transitional boundary layer show important similarities with the sinuous streak instability observed in the near-wall region of a turbulent boundary layer (see Jeong *et al.* 1997; Schoppa & Hussain 1997; Jiménez & Pinelli 1999).

REFERENCES

ACARLAR, M. S. & SMITH, C. R. 1987 A study of hairpin vortices in a laminar boundary layer. Part 2. Hairpin vortices generated by fluid injection. *J. Fluid Mech.* **175**, 43–68.

ANDERSSON, P., BERGGREN, M. & HENNINGSON, D. S. 1999 Optimal disturbances and bypass transition in boundary layers. *Phys. Fluids* **11**, 134–150.

ANDERSSON, P., BRANDT, L., BOTTARO, A. & HENNINGSON, D. S. 2001 On the breakdown of boundary layers streaks. *J. Fluid Mech.* **428**, 29–60.

ASAI, M., MINAGAWA, M. & NISHIOKA, M. 1999 Instability and breakdown of three-dimensional high-shear layer associated with a near-wall low-speed streak. In *Proc. IUTAM Symp.* (ed. H. F. Fasel & W. S. Saric), pp. 269–274. Springer.

ASAI, M., MINAGAWA, M. & NISHIOKA, M. 2002 The instability and breakdown of near-wall low-speed streaks. *J. Fluid Mech.* **455**, 289–314.

BAKCHINOV, A. A., GREK, G. R., KLINGMANN, B. G. B. & KOZLOV, V. V. 1995 Transition experiments in a boundary layer with embedded streamwise vortices. *Phys. Fluids* **7**, 820–832.

BAKE, S., FERNHOLZ, H. H. & KACHANOV, Y. S. 2000 Resemblence of K- and N-regimes of boundary-layer transition at late stages. *Eur. J. Mech.* B/*Fluids* **19**, 1–22.

BERLIN, S. & HENNINGSON, D. S. 1999 A nonlinear mechanism for receptivity of free-stream disturbances. *Phys. Fluids* **11**, 3749–3760.

BERLIN, S., WIEGEL, M. & HENNINGSON, D. S. 1999 Numerical and experimental investigations of oblique boundary layer transition. *J. Fluid Mech.* **393**, 23–57.

BERTOLOTTI, F. P., HERBERT, T. & SPALART, P. R. 1992 Linear and nonlinear stability of the Blasius boundary layer. *J. Fluid Mech.* **242**, 441–474.

BRANDT, L., HENNINGSON, D. S. & PONZIANI, D. 2002 Weakly non-linear analysis of boundary layer receptivity to free-stream disturbances. *Phys. Fluids* **14**, 1426–1441.

BUTLER, K. M. & FARRELL, B. F. 1992 Three-dimensional optimal perturbations in viscous shear flow. *Phys. Fluids* A **4**, 1637–1650.

ELLINGSEN, T. & PALM, E. 1975 Stability of linear flow. *Phys. Fluids* **18**, 487–488.

ELOFSSON, P. A. & ALFREDSSON, P. H. 1998 An experimental study of oblique transition in plane Poiseuille flow. *J. Fluid Mech.* **358**, 177–202.

ELOFSSON, P. A., KAWAKAMI, M. & ALFREDSSON, P. H. 1999 Experiments on the stability of streamwise streaks in plane Poiseuille flow. *Phys. Fluids* **11**, 915–930.

HERBERT, T. 1983 Secondary instability of plane channel flow to subharmonic three-dimensional disturbances. *Phys. Fluids* **26**, 871–874.

HERBERT, T. 1988 Secondary instability of boundary-layers. *Annu. Rev. Fluid Mech.* **20**, 487–526.

HULTGREN, L. S. & GUSTAVSSON, L. H. 1981 Algebraic growth of disturbances in a laminar boundary layer. *Phys. Fluids* **24**, 1000–1004.

JACOBS, R. J. & DURBIN, P. A. 2001 Simulations of bypass transition. *J. Fluid Mech.* **428**, 185–212.

JEONG, J., HUSSAIN, F., SCHOPPA, W. & KIM, J. 1997 Coherent structures near the wall in a turbulent channel flow. *J. Fluid Mech.* **332**, 185–214.

JIMÉNEZ, J. & PINELLI, A. 1999 The autonomous cycle of near wall turbulence. *J. Fluid Mech.* **389**, 335–359.

JIMÉNEZ, J. & SIMENS, M. P. 2001 Low dimensional dynamics of a turbulent wall flow. *J. Fluid Mech.* **435**, 81–91.

KACHANOV, Y. S. 1994 Physical mechanism of laminar boundary-layer transition. *Annu. Rev. Fluid Mech.* **26**, 411–82.

KACHANOV, Y. S., KOZLOV, V. V. & LEVCHENKO, V. Y. 1977 Nonlinear development of a wave in a boundary layer. *Izv. Akad. Nauk SSSR Mekh. Zhid. Gaza* **3**, 49–58 (in Russian).

KAWAHARA, G., JIMÉNEZ, J., UHLMANN, M. & PINELLI, A. 1998 The instability of streaks in near-wall turbulence. *Annual Research Briefs*, NASA-Stanford University Center for Turbulence Research. pp. 155–170.

KENDALL, J. M. 1985 Experimental study of disturbances produced in a pre-transitional laminar boundary layer by weak free-stream turbulence. *AIAA Paper* 85-1695.

KIM, H. T., KLINE, S. J. & REYNOLDS, W. C. 1971 The production of turbulence near a smooth wall in a turbulent boundary layer. *J. Fluid Mech.* **50**, 133–160.

KIM, J., MOIN, P. & MOSER, R. 1987 Turbulence statistics in fully developed channel flow. *J. Fluid Mech.* **177**, 133–166.

KLEBANOFF, P. S. 1971 Effect of free-stream turbulence on the laminar boundary layer. *Bull. Am. Phys. Soc.* **10**, 1323.

KLEBANOFF, P. S., TIDSTROM, K. D. & SARGENT, L. M. 1962 The three-dimensional nature of boundary layer instability. *J. Fluid Mech.* **12**, 1–34.

LANDAHL, M. T. 1975 Wave breakdown and turbulence. *SIAM J. Appl. Maths* **28**, 735.

LANDAHL, M. T. 1980 A note on an algebraic instability of inviscid parallel shear flows. *J. Fluid Mech.* **98**, 243–251.

LAURIEN, E. & KLEISER, L. 1989 Numerical simulation of boundary-layer transition and transition control. *J. Fluid Mech.* **199**, 403–440.

LECUNFF, C. & BOTTARO, A. 1993 Linear stability of shear profiles and relation to the secondary instability of the Dean flow. *Phys. Fluids* A **5**, 2161–2171.

LI, F. & MALIK, M. R. 1995 Fundamental and subharmonic secondary instabilities of Görtler vortices. *J. Fluid Mech.* **297**, 77–100.

LIU, W. & DOMARADZKI, A. J. 1993 Direct numerical simulation of transition to turbulence in Görtler flows. *J. Fluid Mech.* **246**, 267–299.

LUCHINI, P. 2000 Reynolds-number independent instability of the boundary layer over a flat surface. Part 2: Optimal perturbations. *J. Fluid Mech.* **404**, 289–309.

LUNDBLADH, A., BERLIN, S., SKOTE, M., HILDINGS, C., CHOI, J., KIM, J. & HENNINGSON, D. S. 1999 An efficient spectral method for simulation of incompressible flow over a flat plate. *Tech. Rep.* KTH/MEK/TR–99/11–SE. KTH. Department of Mechanics, Stockholm.

MALIK, M. R., ZANG, T. A. & HUSSAINI, M. Y. 1985 A spectral collocation method for the Navier-Stokes equations. *J. Comput. Phys.* **61**, 64–88.

MATSUBARA, M. & ALFREDSSON, P. H. 2001 Disturbance growth in boundary layers subjected to free stream turbulence. *J. Fluid Mech.* **430**, 149–168.

MEYER, D. G. W., RIST, U., BORODULIN, V. I., GAPONENKO, V. R., KACHANOV, Y. S., LIAN, Q. X. & LEE, C. B. 1999 Late-stage transitional boundary-layer structures. Direct numerical simulation and experiment. In *Proc. IUTAM Symp.* (ed. H. F. Fasel & W. S. Saric), pp. 167–172. Springer.

NORDSTRÖM, J., NORDIN, N. & HENNINGSON, D. S. 1999 The fringe region technique and the Fourier method used in the direct numerical simulation of spatially evolving viscous flows. *SIAM J. Sci. Comput.* **20**, 1365–1393.

ORR, W. M. F. 1907 The stability or instability of the steady motions of a perfect liquid and of a viscous liquid. Part I: A perfect liquid. Part II: A viscous liquid. *Proc. R. Irish Acad.* A **27**, 9–138.

PARK, D. S. & HUERRE, P. 1995 Primary and secondary instabilities of the asymptotic suction boundary layer on a curved plate. *J. Fluid Mech.* **283**, 249–272.

PHILLIPS, O. M. 1969 Shear-flow turbulence. *Annu. Rev. Fluid Mech.* **1**, 245–264.

RAYLEIGH, LORD 1880 On the stability of certain fluid motions. *Proc. Math. Soc. Lond.* **11**, 57–70.

REDDY, S. C. & HENNINGSON, D. S. 1993 Energy growth in viscous channel flows. *J. Fluid Mech.* **252**, 209–238.

REDDY, S. C., SCHMID, P. J., BAGGETT, J. S. & HENNINGSON, D. S. 1998 On the stability of streamwise streaks and transition thresholds in plane channel flows. *J. Fluid Mech.* **365**, 269–303.

RIST, U. & FASEL, H. 1995 Direct numerical simulation of controlled transition in a flat-plate boundary layer. *J. Fluid Mech.* **298**, 211–248.

SANDHAM, N. D. & KLEISER, L. 1992 The late stages of transition to turbulence in channel flow. *J. Fluid Mech.* **245**, 319–348.

SCHLICHTING, H. 1933 Berechnung der anfachung kleiner störungen bei der plattenströmung. *Z. Angew. Math. Mech.* **13**, 171–174.

SCHMID, P. & HENNINGSON, D. S. 1992 A new mechanism for rapid transition involving a pair of oblique waves. *Phys. Fluids* A **4**, 1986–1989.

SCHMID, P. J. & HENNINGSON, D. S. 2001 *Stability and Transition in Shear Flows*. Springer.

SCHOPPA, W. & HUSSAIN, F. 1997 Genesis and dynamics of coherent structures in near-wall turbulence: a new look. In *Self-Sustaining Mechanisms of Wall Turbulence* (ed. R. L. Panton), chap. 7, pp. 385–422. Computational Mechanics Publications, Southampton.

SCHUBAUER, G. B. & SKRAMSTAD, H. F. 1947 Laminar boundary layer oscillations and the stability of laminar flow. *J. Aero. Sci.* **14**, 69–78.

SKOTE, M. 2001 Studies of turbulent boundary layer flow through direct numerical simulation. PhD thesis, Royal Institute of Technology, Stockholm, Sweden.

SKOTE, M., HARITONIDIS, J. H. & HENNINGSON, D. S. 2002 Varicose instabilities in turbulent boundary layers. *Phys. Fluids* **14**, 2309–2323.

SOMMERFELD, A. 1908 Ein beitrag zur hydrodynamischen erklärung der turbulenten flüssigkeitbewegungen. In *Atti. del 4. Congr. Internat. dei Mat. III, Roma*, pp. 116–124.

SPALART, P. R. & YANG, K. 1987 Numerical study of ribbon induced transition in Blasius flow. *J. Fluid Mech.* **178**, 345–365.

SWEARINGEN, J. D. & BLACKWELDER, R. F. 1987 The growth and breakdown of streamwise vortices in the presence of a wall. *J. Fluid Mech.* **182**, 255–290.

TOLLMIEN, W. 1929 Über die entstehung der turbulenz. *Nachr. Ges. Wiss. Göttingen 21–24* (English translation *NACA TM* 609, 1931).

WALEFFE, F. 1995 Hydrodynamic stability and turbulence: Beyond transients to a self-sustaining process. *Stud. Appl. Maths* **95**, 319–343.

WALEFFE, F. 1997 On a self-sustaining process in shear flows. *Phys. Fluids* A **9**, 883–900.

WESTIN, K. J. A., BOIKO, A. V., KLINGMANN, B. G. B., KOZLOV, V. V. & ALFREDSSON, P. H. 1994 Experiments in a boundary layer subject to free-stream turbulence. Part 1: Boundary layer structure and receptivity. *J. Fluid Mech.* **281**, 193–218.

WILLIAMS, D. R., FASEL, H. & HAMA, F. R. 1984 Experimental determination of the three-dimensional vorticity field in the boundary-layer transition process. *J. Fluid Mech.* **149**, 179–203.

WU, X., JACOBS, R. G., HUNT, J. C. R. & DURBIN, P. A. 1999 Simulation of boundary layer transition induced by periodically passing wakes. *J. Fluid Mech.* **398**, 109–153.

WUNDROW, D. W. & GOLDSTEIN, M. E. 2001 Effect on a laminar boundary layer of small-amplitude streamwise vorticity in the upstream flow. *J. Fluid Mech.* **426**, 229–262.